

Review

# Nickel Alloying in Carbon Steel: Fundamentals and Applications

Hardy Mohrbacher <sup>1,2,\*</sup>  and Andreas Kern <sup>3</sup><sup>1</sup> NiobelCon BV, Swaenebeecklaan 5, 2979 Schilde, Belgium<sup>2</sup> KU Leuven, MTM, De Croylaan, 3001 Heverlee, Belgium<sup>3</sup> Thyssenkrupp Steel Europe AG, Kaiser-Wilhelm-Str. 100, 47166 Duisburg, Germany

\* Correspondence: hm@niobelcon.net

**Abstract:** Nickel is an important and widely used alloying element in carbon steels. Some of its prominent metallurgical effects in these steels are moderate solid solution strengthening, mild hardenability and, importantly, a strong promotion of toughness, especially at low temperatures. The first uses of nickel as an alloying element in commercial steel production date back to the early 20th century. The aim of the current review is to give the reader a thorough and concise overview of nickel functionalities relevant to modern carbon steel production. The interaction of nickel with other alloying elements and processing conditions is also considered. Examples will be given demonstrating the advantages of nickel alloying in selected steel grades and applications.

**Keywords:** solid solution; transformation; strengthening; toughness; welding; fatigue; corrosion; hot shortness; HSLA steel; cryogenic steel

## 1. Introduction

Nickel belongs to the group of industrial metals and is used in a wide variety of commercial and industrial applications. The metal is extracted by large-scale mining operations to an annual amount of 2.4 million metric tons (reference year 2020). According to current growth scenarios, the global first-use nickel consumption is expected to nearly double, reaching 4.7 million tons by the year 2030. The global demand of nickel is dominated by stainless steel production (currently 73%) while battery applications (currently 8%) are mainly driving its future growth rate [1]. Carbon steel production, however, consumes only about 3% of the annual nickel volume.

Nickel (atomic number 28) is part of the transition metals range in the periodic table [2]. Like its direct neighbors, iron (atomic number 26) and cobalt (atomic number 27), nickel is ferromagnetic with a Curie temperature of 354 °C. Pure nickel is a silvery-white metal with a density of 8.91 g/cm<sup>3</sup>. The lattice structure is face-centered cubic (lattice parameter  $a = 352.4$  pm) showing no allotropy. Accordingly, Ni does not undergo any change in its face-centered cubic crystal structure under atmospheric pressure up to its melting point, contrary to iron which transforms from a face-centered cubic (fcc) structure at higher temperatures to a body-centered cubic (bcc) structure at lower temperatures.

Nickel alloying is strategically important in several carbon steel product families used for demanding applications. Often it is added to amounts below 1 wt.%, yet in selected steel grades the nickel alloy level reaches 9 wt.%. Nickel, through its various metallurgical effects, facilitates processing and enhances component performance during service. Therefore, nickel cannot easily be substituted by other alloys despite frequent attempts to do so due to its price volatility in the metals trading market. On the other hand, using nickel alloying in an optimum way can deliver benefits clearly justifying its alloy cost.

Nickel has been one of the first special alloying elements in steel production and has been used since the early 20th century [3]. Principal metallurgical understanding of it has been developed and published since then based on the means and needs of that time. Starting from this established understanding of nickel's metallurgical functionality



**Citation:** Mohrbacher, H.; Kern, A. Nickel Alloying in Carbon Steel: Fundamentals and Applications. *Alloys* **2023**, *2*, 1–28. <https://doi.org/10.3390/alloys2010001>

Academic Editor: Kenta Yamanaka

Received: 13 December 2022

Revised: 4 January 2023

Accepted: 6 January 2023

Published: 11 January 2023



**Copyright:** © 2023 by the authors. Licensee MDPI, Basel, Switzerland. This article is an open access article distributed under the terms and conditions of the Creative Commons Attribution (CC BY) license (<https://creativecommons.org/licenses/by/4.0/>).

in carbon steels, the current review provides deeper insights and summarizes recent findings on how nickel helps improve the properties as well as the processing of modern steels. The aim is to give the reader a thorough and concise overview of relevant nickel functionalities in carbon steels including understanding from most recent research activities. The review concludes with representative examples demonstrating the implementation of nickel alloying in advanced steel products using modern processing technologies.

## 2. Fundamental Metallurgical Effects of Nickel in Carbon Steels

### 2.1. Nickel Effects on the Transformation Behavior

Due to the similarity in principal properties, nickel and iron form a substitutional solid solution when mixed together. The Fe–Ni binary-phase diagram, which principally represents the possible phase formation in steels alloyed with nickel indicates the stabilization of the austenitic (fcc) phase in Ni-alloyed steel towards lower temperatures (Figure 1a). Two-phase ferritic-austenitic microstructures exist at room temperature when the Ni contents exceed approximately 15 wt.%. Bainite or martensite formation is promoted upon down-cooling as a result of the decreasing transformation temperature with increasing nickel content. Above 6 wt.% Ni content, diffusion-controlled transformation processes are fully suppressed, resulting in martensite transformation. In the presence of carbon, phase fields are somewhat shifted but, principally, the effects of nickel on the transformation behavior remain similar. Experimentally determined  $A_{c1}$  and  $A_{c3}$  temperatures are shown in Figure 1b as a function of the nickel content in a 0.1 wt.% carbon-containing steel [4]. The influence of nickel is obviously stronger on the  $A_{c3}$  temperature than on the  $A_{c1}$  temperature. These temperatures are important with regard to re-austenitizing and tempering treatments.

The activation energy for the diffusion of nickel atoms in iron is rather high, so that the diffusion coefficient of nickel is generally low and comparable to the self-diffusion of iron [5]. Therefore, equilibration of concentration variations can be achieved only during long holding times at high temperature. However, nickel diffuses faster in bcc iron than in fcc iron. This difference causes a hysteresis in the transformation behavior between cooling and heating cycles and becomes pronounced for Ni contents above approximately 5%. Martensite transformation commences during down-cooling when passing the  $M_s$  (martensite-start) temperature. Before reaching  $M_f$  (martensite-finish) temperature, bcc and fcc phases coexist; however, the nickel concentration in either phase can be assumed to be nearly equal due to the very slow diffusion. However, when reheating above the  $\gamma_s$  (austenite-start) temperature into the region of coexisting fcc and bcc phases, nickel can partition into austenite, provided the holding time is sufficiently long. Such nickel-enriched crystallites can finally survive as metastable retained austenite phases when cooling back to ambient temperature. In technical steel alloys, carbon and manganese also partition to these austenite islands providing additional stabilization. The retained austenite fraction present in carbon steels after heat treatment enables a transformation-induced plasticity (TRIP) effect and makes an important contribution to enhanced formability and low temperature toughness, as will be discussed later (see Section 2.6).

In the high-temperature range, the Fe–Ni binary alloy comprises a peritectic reaction such as the Fe–C binary alloy. Solidification from the liquid phase can proceed along various phase transformation scenarios (Figure 1c) [6]. For lower nickel additions (<3.4 wt.%), with a respectively low carbon content, solidification occurs entirely as  $\delta$ -ferrite, subsequently transforming to austenite. The final transformation starts by nucleation of  $\alpha$ -ferrite at the austenite grain boundaries and subsequent growth. The size of these ferrite grains depends on the degree of undercooling controlled by the Ni content and the cooling rate. At higher nickel content the austenite phase either transforms by nucleation of grain boundary ferrite or by diffusionless transformation into martensite below the  $M_s$  temperature. In the latter case, the boundaries of the prior columnar austenite grains will be maintained with the martensite substructure developing inside this boundary. Especially after direct solidification from liquid to austenite, impurities such as sulfur and

phosphorous segregated to the austenite grain boundary also decorate the prior austenite grain boundary in the final martensitic microstructure. This is not the case when ferrite nucleation and growth erase the prior austenite boundaries in steels with lower nickel content. Additionally, dilatational stresses originating from the martensite transformation act on the prior austenite grain boundaries. The resulting embrittlement of such boundaries can cause intergranular cracking and is relevant to the performance of higher-nickel alloyed steels in as-cast condition as well as after fusion welding. The removal of this detrimental effect requires dedicated heat treatment.

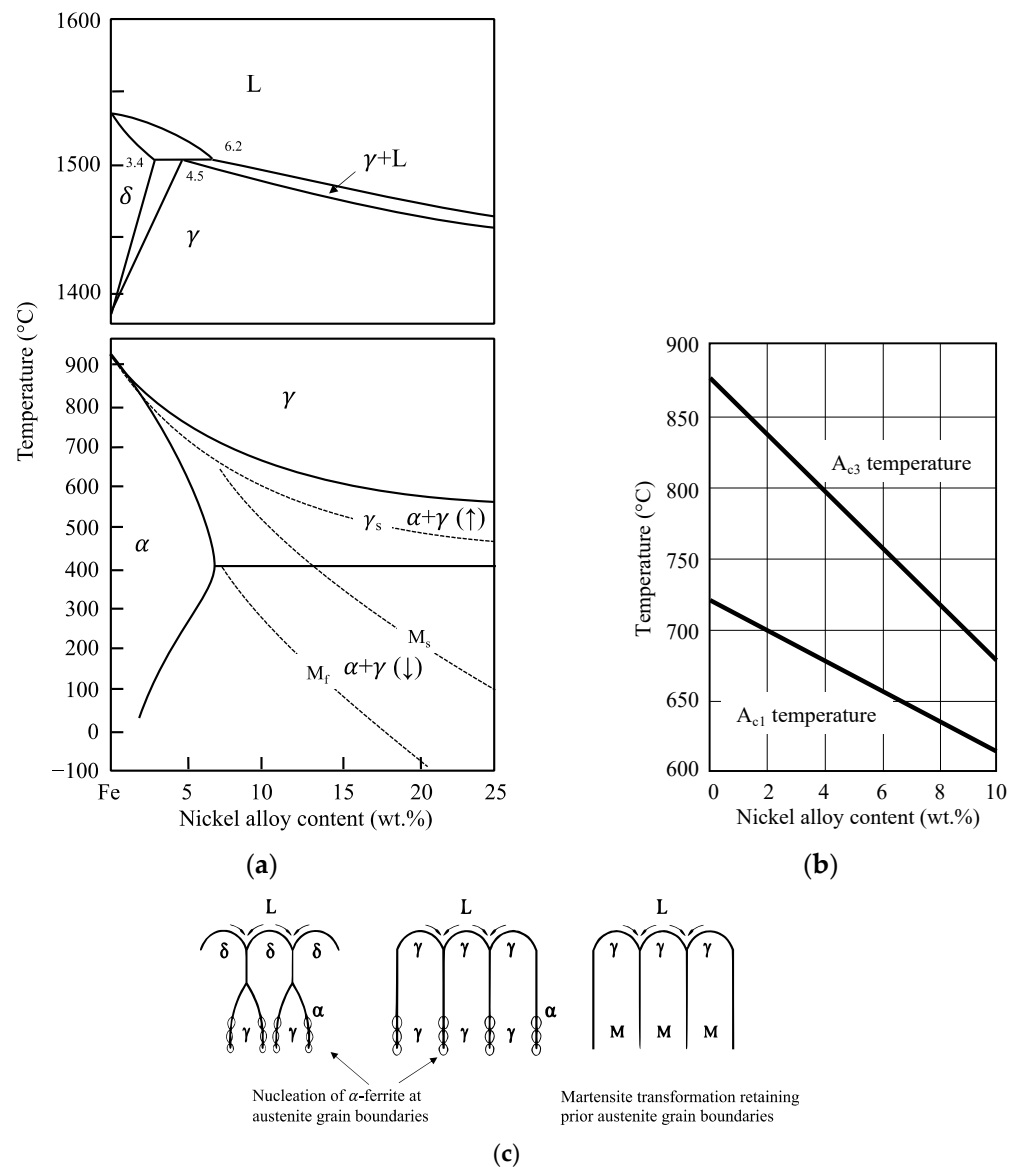


**Figure 1.** (a) Phase diagram of binary Fe–Ni alloy (Composed from data in [7–9]); (b) influence of nickel alloying on the transformation temperature of 0.1 wt.% carbon steel upon re-austenitizing using data from [4]; (c) solidification scenarios for carbon steels with increasing nickel content (Reprinted from Ref. [6]).

## 2.2. Nickel Interaction with Carbon

Nickel can form a carbide species with the composition  $\text{Ni}_3\text{C}$ . The decomposition of the metastable  $\text{Ni}_3\text{C}$  carbide into Ni and C starts at a temperature of around  $465\text{ }^\circ\text{C}$  and is accompanied by a thermal effect  $-\Delta H \approx 10\text{ kJ/mol}$  [10]. However, due to its low affinity to carbon, nickel carbide does not form in steel. In ternary Fe–C–Ni alloys, the diffusivities of nickel and carbon are mutually enhanced. Small amounts of nickel dissolved in iron

carbide (cementite) facilitate its decomposition, which results in graphite formation during long holding periods at high pearlite temperature. The graphite-promoting effect of nickel is prominent in cast iron alloys but not relevant to carbon steels. As early as the year 1924 it had been reported that nickel lowers the pearlite formation temperature and lowers the eutectoid carbon content [11]. Quantitatively, the addition of 1 wt.% Ni reduces the pearlite formation temperature by about 15 K and lowers the eutectoid carbon content by around 0.04 wt.% [12]. However, nickel does not refine the pearlite lamellar structure beyond that provoked by the undercooling effect [13]. Accordingly, nickel alloying to low carbon steel increases the phase fraction of pearlite, as was observed for a 0.17 wt.%C steel in which the pearlite phase fraction linearly increased from 0.2 to 0.3 when adding up to 3 wt.% Ni [14].

Like silicon, nickel raises the activity of carbon in steel, which also affects the solubility of micro-alloy carbides at low level. The results of Eckstein et al. [15] indicate that the dissolution temperature of niobium carbo-nitride is increased by only about 5 K when adding 0.5 wt.%Ni to carbon steel. Manganese, molybdenum, and chromium on the contrary reduce the niobium carbonitride dissolution temperature by a similar magnitude at 0.5 wt.% addition levels. Sharma et al. [16] derived interaction parameters for nickel and other common alloying elements allowing the correction of the niobium solubility product. However, as the magnitude of the nickel effect on the solubility of micro-alloy carbides in relevant steel compositions is rather small, it has no significant consequences regarding practical soaking treatments. On the other hand, an enhanced carbon activity by nickel could promote micro-alloy precipitation at lower austenite temperature.

### 2.3. Transformation Kinetics and Hardenability of Nickel Alloyed Carbon Steels

The significant extension of the austenite phase field by nickel alloying in combination with its low diffusivity in the austenite lattice delays the austenite-to-ferrite transformation towards lower temperature or extended times. The resulting undercooling causes an increased ferrite nucleation rate and decreased ferrite growth rate leading to a general refinement of the ferrite microstructure. However, Kosazu [17] has reported that the refining effect of nickel alone and under slow cooling rates is rather modest. Accelerated cooling from temperatures above  $A_{r3}$  induces a similar undercooling effect and refinement mechanisms. The nickel alloy effect in combination with that of accelerated cooling can thereby act in synergy (Figure 2a) [17,18]. The excessive application of both parameters, i.e., Ni alloying and accelerated cooling might cause, however, the formation of undesirable coarse bainite structures during the transformation from equiaxed austenite. This is related to the circumstance that only preferential austenite grain boundaries can nucleate ferrite grains. Enhancing the heterogeneity in austenite by controlled deformation below the recrystallization temperature, however, provides a much larger number of ferrite nucleation sites, avoiding the formation of coarse-grained bainitic features (Figure 2b).

These austenite heterogeneities represented by total grain boundary area and intergranular deformation bands are quantitatively described by the  $S_V$  parameter, i.e., effective grain boundary area per unit volume. Controlled austenite deformation in combination with accelerated cooling produces very fine-grained ferrite, resulting in high yield strength and low ductile-to-brittle transition temperature upon impact loading. However, particularly in heavy-gauged products, it is often not possible to achieve a high degree of controlled deformation in the central area. Furthermore, the achievable cooling rates are comparably low. Thus, nickel alloying can effectively help to improve mechanical properties in sections where such inferior processing conditions prevail.

With increasing nickel alloy content, pearlite and subsequently bainite transformation is progressively suppressed, finally leading to full martensite formation. The maximum transformation rate for combined pearlite and bainite formation decreases with increasing nickel content. In steels with more than 3 wt.% Ni it becomes therefore difficult to separate pearlite from bainite formation. The influence of increasing nickel alloy content up to 9 wt.% Ni on the transformation behavior of low-carbon structural steels is exemplarily demonstrated by the CCT curves in Figure 3.

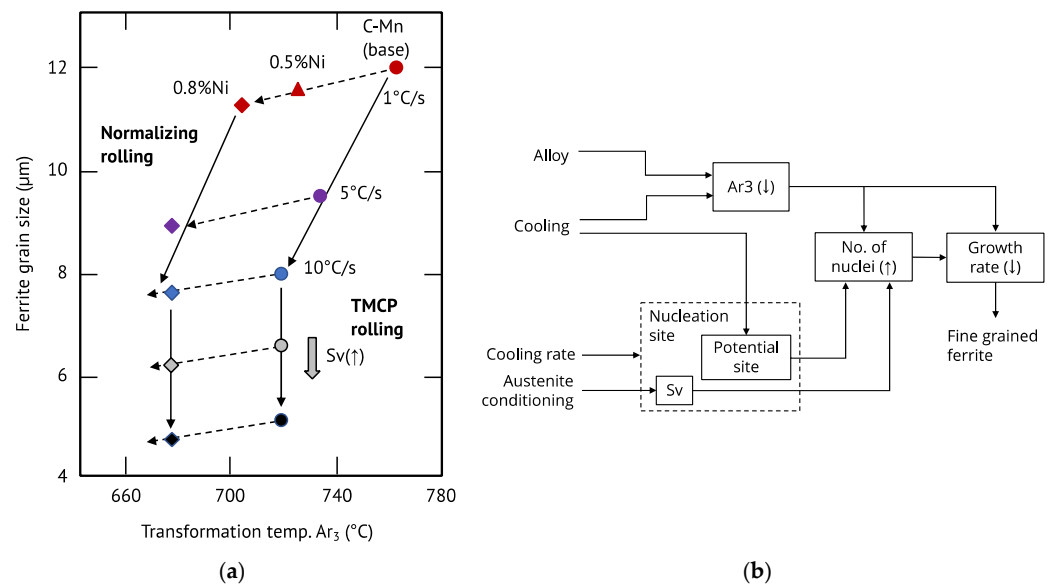


**Figure 2.** (a) Example of nickel alloy effect and processing conditions on achievable ferrite grain size in low-carbon plate steel; (b) principles of achieving fine ferrite grain size by alloying and processing of carbon steels.

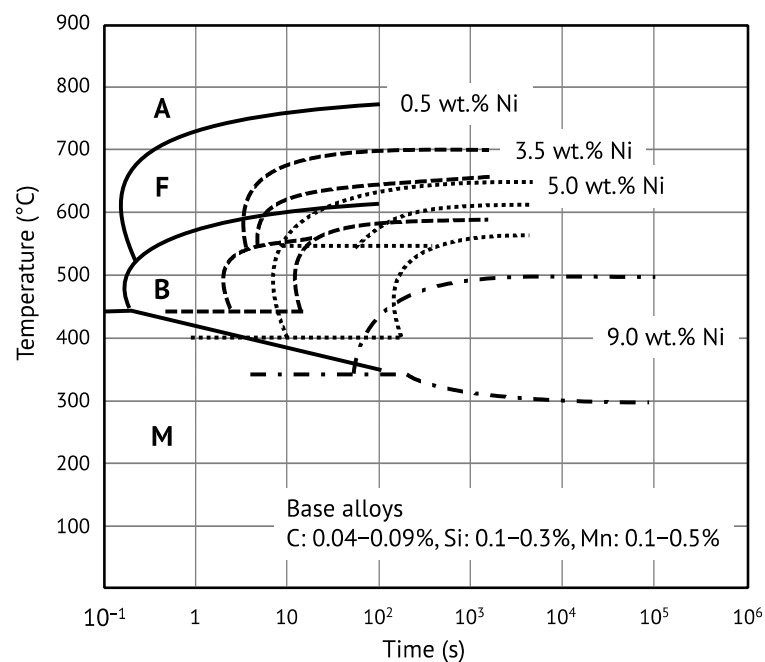


**Figure 3.** CCT diagrams (austenitizing at 800–900  $^{\circ}\text{C}$ ) demonstrating the effect of Ni on the transformation behavior of low-carbon structural steels (Reprint from Ref. [19]).

The martensite-start ( $M_s$ ) temperature decreases with 17–19 K per weight percent nickel added [20]. It is commonly understood that martensite transformation is an athermal process (i.e., it does not require thermal activation) that cannot be suppressed. However, it has been known for a long time that isothermal formation of martensite is also feasible. Borgenstam and Hillert [21] have reviewed these early studies regarding the kinetics of isothermal martensite transformation. The activation energy was estimated to be in the range of 7 to 80 kJ/mol for different alloy systems. While activation energies on the lower side should rather be related to growth mechanisms involving dislocation movements, those on the higher side would quite well agree with the activation energy required for carbon diffusing away from a growing bcc plate within the undercooled austenite. The

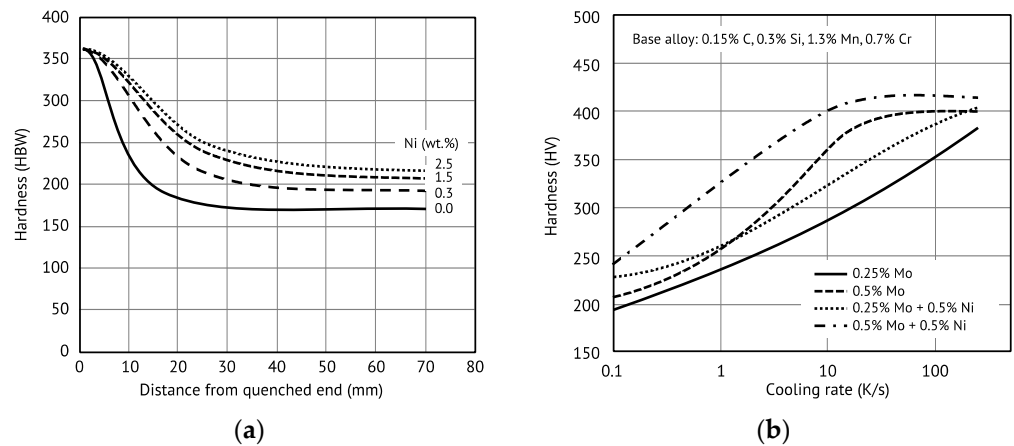
practical relevance of isothermal martensite formation has been concisely discussed by Villa and Somers [22] in the light of innovative cryogenic treatments on high-performance steels. Their results, using 15–17 wt.% Cr steel alloys, reveal that increasing the nickel content from 2 to 7 wt.% drastically reduces the athermal martensite share when fast cooling the alloy from room temperature to  $-196\text{ }^{\circ}\text{C}$  followed by up-quenching in water [23]. However, slow isochronal heating from the cryogenic temperature, or isothermal holding, ideally in the range from  $-80$  to  $-40\text{ }^{\circ}\text{C}$ , produces a large volume fraction of isothermal martensite. The activation energy for the formation of this suppressible martensite was found to increase in the range of 0 to 30 kJ/mol depending on the interstitial (C, N) content, however without an apparent influence by the nickel or chrome content [23]. It can be inferred that the nickel alloy content primarily interferes with the nucleation of athermal martensite.

The multiplying factor of nickel quantifying its hardenability effect is moderate and comparable to that of silicon but smaller than those of manganese, molybdenum, and chromium [12]. However, nickel alloying at reasonably low addition levels can significantly enhance the efficiency of other alloying elements for generating strong microstructures by enabling synergy effects. To understand the principle of these synergies, the different mechanisms providing hardenability must be considered:

- (a) Delay of phase transformation by lowering the  $A_{r1}$  and  $A_{r3}$  temperatures
- (b) Solute drag on the phase transformation front
- (c) Obstruction of carbon diffusion
- (d) Suppression of grain boundary ferrite nucleation.

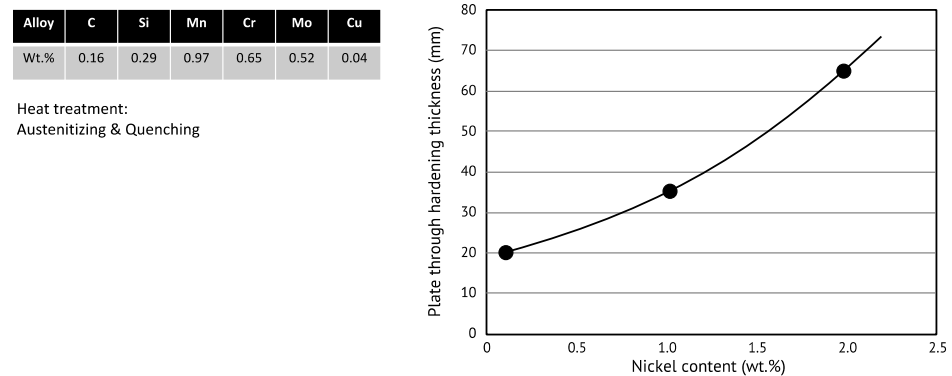
Nickel and manganese, extending the austenite phase field, act by mechanism (a). The solute drag mechanism (b) is most pronounced for large alloy atoms such as niobium, molybdenum, and titanium. The obstruction of carbon diffusion (c), retarding pearlite formation, is promoted by chromium and also by other carbide formers (Nb, Ti, V, Mo). Solute boron strongly segregates to the austenite grain boundary, lowering its energy, thus, obstructing ferrite nucleation by mechanism (d). The magnitude of mechanism (b) is influenced by the diffusivity of the respective drag exerting solutes at the temperature of phase transformation. Since nickel lowers the  $A_{r3}$  temperature, irrespective of the cooling rate, the diffusivity of these elements is inherently reduced. Regarding mechanism (d), the segregation of boron at the austenite grain boundary relies on the vacancy flux dragging boron (and also Mo, Nb) towards the boundary. As the austenite temperature decreases, vacancies flow from the grain interior to the boundary which acts as a sink. Again, the lower transformation temperature caused by nickel alloying enhances this non-equilibrium segregation mechanism by a stronger vacancy flux. Accordingly, for production routes where sufficiently high cooling rates can be guaranteed across the entire thickness, nickel alloying may not be essential for hardenability. In heavy-gauged products, however, the cooling rate in the center region is naturally limited and nickel alloying on top of the applicable maximum manganese content becomes relevant for retarding the transformation.

Figure 4a illustrates the hardenability as a function of the nickel content in structural steel grade S460 by comparing Jominy curves. It is evident that the hardenability increase is most prominent for smaller nickel additions. At higher nickel content the increasing effect on hardenability levels off. The hardness increase occurs along with a gradual shift from a ferritic–pearlitic towards a bainitic–martensitic microstructure. Figure 4b demonstrates the synergy between Ni and Mo in the function of the cooling rate. The molybdenum-related hardenability is not very pronounced at low cooling rates, irrespective of the added amount. Nickel alloying, on the contrary, provides better hardenability at these low cooling rates. At higher cooling rates the hardenability effect by 0.5 wt.% Mo is saturating. Combined alloying of Ni and Mo to 0.5 wt.%, each, provides very good hardenability, one which is better than the sum of the individual alloy effects for cooling rates up to 10 K/s.



**Figure 4.** (a) Jominy curves indicating the effect of increasing Ni content on the hardenability of grade S460 low-carbon structural steel; (b) hardness in function of defined cooling rate by dilatometer testing demonstrating hardenability performance of molybdenum, nickel and synergies between both.

The nickel-induced lowering of the transformation temperature and the associated increase in the driving force for the bainitic transformation results in a refinement of the bainite package and block size, which noticeably supports the hardness-increasing effect of nickel [24,25]. Lowering the carbon content and increasing the nickel addition promotes this refinement. The resulting enhanced density of block boundaries and Bain variant pairs leads to a high hardness even at the low cooling rates encountered in the center section of heavy-gauged products. Alloying 2 wt.% Ni to a water-quenched high-strength steel allows the through-hardenable plate thickness to be more than tripled, as demonstrated by Figure 5.



**Figure 5.** Impact of nickel alloying on through-thickness hardening in a heat-treatable steel.

#### 2.4. Solute Atom Effects of Nickel

The variation in the lattice parameters of austenite and ferrite, with the addition of an alloying element, strongly depends upon the relative difference in atomic radius between iron and the alloying element: the so-called misfit parameter. Nickel, like manganese and chromium, has an atomic size rather similar to that of iron. Accordingly, it has a small effect on the lattice parameter in bcc iron. Leslie [26] and, more recently, Hagi [27] have provided quantitative data for this effect. Host lattice distortion by nickel alloying is accordingly rather small. Nevertheless, solute nickel has a quite significant effect on the Young's ( $E$ ) and shear ( $G$ ) moduli of bcc iron. Ledbetter and Reed [28] derived relationships describing the influence of nickel content  $C_{Ni}$  in wt.% as

$$E \text{ (GPa)} = 205 - 1.75 \cdot C_{Ni} \quad (1)$$

$$G \text{ (GPa)} = 81 - 1.12 \cdot C_{Ni} \quad (2)$$

which can have important consequences, for instance, regarding the fracture behavior of carbon steels. Accordingly, Morris et al. [29] pointed out that in a Fe-12 wt.%Ni alloy the ideal cleavage and shear strengths are respectively more than 10% and 16% below that of pure Fe, and a ferritic alloy containing more than 32 wt.% Ni would become virtually immune to cleavage.

The interaction of alloying elements in substitutional solution with defects and interstitials is controlled by the lattice strain caused by the alloying atom. It is reasonable to assume that the solid solution strengthening effect should correlate with the misfit parameter. The normalized lattice distortion is proportional to the concentration of the substitutional element and has been reported to be in the range of  $1.65\text{--}2.31 \times 10^{-4}$  per at.% for nickel which is very similar to that for manganese ( $1.80\text{--}2.30 \times 10^{-4}$  1/at.%) and larger than that for chromium ( $1.20\text{--}1.90 \times 10^{-4}$  per at.%) [27]. In comparison, larger-sized substitutional atoms such as molybdenum or vanadium cause much bigger misfits, in the range of  $5.21\text{--}8.36 \times 10^{-4}$  per at.% and  $3.53\text{--}4.04 \times 10^{-4}$  per at.% [27]. While chromium, vanadium, and molybdenum fit quite well to a linear correlation between misfit parameter and solid solution strengthening, nickel and manganese strengthen bcc iron more than their misfit parameter suggests [30]. Under tensile test conditions at ambient temperature (23 °C) and low strain rate ( $10^{-4}$  s<sup>-1</sup>) around a 20 MPa yield strength increase per at.% Ni alloy addition can be achieved by solid solution strengthening [30]. On the other hand, binary iron alloys containing Ni (and similarly Mn, Al and Si) exhibit solid solution softening below a temperature of 250 K [30–32]. Solid solution softening has been attributed to a decrease in the kink-pair nucleation energy with increasing solute content. Following the original suggestion by Weertman, a solute atom misfit center would interact with a dislocation, helping to pull it out of the Peierls energy valley [33,34]. This interpretation, however, does not assume a direct influence of nickel on the Peierls stress. The experimental results of Hildebrandt and Dickenscheid [35] prove that the activation energy for slip in Fe–Ni alloys is reduced relative to pure iron. This difference increases with the nickel content over the investigated alloy range of up to 3 at.% and also increases the further that temperature decreases below ambient. The authors attributed this behavior to a disturbance in the iron matrix caused by the change of the lattice parameter and elastic modulus due to nickel alloying. Furthermore, it was argued that nickel fills the incomplete 3d electron shell of iron, thus diminishing the influence of covalent bonding so that more active slip systems are available at low temperature. Chen et al. [36] have presented results on the plastic flow of binary Fe–Ni alloys, which are congruent with those reported in [35]. Their analysis indeed suggests that the Peierls stress decreased from 920 MPa in pure iron to 640 MPa when adding 4 at.% Ni. The temperature dependence of the strain rate sensitivity exposes a local minimum, which shifts towards lower temperatures with increasing nickel content.

Due to its relatively small misfit parameter, high solubility and slow diffusivity in iron, nickel has only a weak tendency for segregating to grain boundaries. This is contrary to solute atoms inducing a larger misfit such as molybdenum or niobium [30,37]. The low binding energy of nickel to the boundary results in a comparably small solute drag effect. Empirical work by Lee [38] indicates that the contribution of nickel in enhancing the activation energy for austenite grain growth is considerably lower than that of molybdenum and also lower than that of chromium. Ab-initio calculations by Hoerner et al. [39] demonstrate a good correlation between the binding energy of solutes to preferential substitutional sites and the activation energy for austenite growth. Accordingly, nickel has a small impact on obstructing the boundary mobility, which is a major factor regarding austenite recrystallization and grain growth. Research by Jin et al. [40], using first-principle calculations, suggests that nickel also has a low binding energy to the bcc–fcc transformation interface. Hence, its solute drag effect on the phase transformation front is also small. Modelling of alloy effects on ferrite growth proceeding from the transformation of austenite by Zurob et al. [41] confirmed a weak interaction of nickel with the interface along with the tendency for carbon to repel nickel from the interface.

High temperature plasticity in ferrite relies on the mobility of dislocations and recovery phenomena. Solute alloy atoms can retard the gliding motion of dislocations by dragging. The climbing motion of dislocations is controlled by vacancy flow towards the dislocation core. Yoshida et al. [42] have argued that the dragging force of solutes on dislocation gliding is determined by the solute misfit parameter and its self-diffusion coefficient. Accordingly, nickel has only a small drag effect which is owed mostly to its limited diffusivity rather than to its small misfit.

The diffusion coefficient of nickel in a highly defective microstructure, however, can be considerably increased as compared to normal lattice diffusion [43]. Enhanced nickel diffusion has been observed, for instance, after cold-working or neutron irradiation [44]. Thereby the activation energy for diffusion of nickel in the highly defective steel microstructure is attributed mainly to the activation energy for vacancy migration. In that case, the already weak obstructive effect of solute nickel on dislocation glide or recovery should be further reduced. Enhanced nickel diffusivity is also promoting nickel partitioning during heat treatment in the temperature range of coexisting ferrite and austenite. This is the case when a defect-rich original microstructure such as martensite is tempered in the inter-critical temperature range resulting in a fraction of metastable retained austenite.

Another plasticity-influencing effect of nickel is related to a change in stacking fault energy (SFE). In fcc metals, such as austenite, stacking faults (SF) are interruptions in the perfect (ABCABC) sequential layering of the (111) crystallographic planes. These faults are formed by either dissociation of a perfect dislocation into two partial dislocations, or by emission of partial dislocations from grain boundaries. The stacking fault energy is required for generating this lattice irregularity. Pure nickel metal has a comparably high stacking fault energy (SFE  $\sim 128$  mJ/m<sup>2</sup>) so that the number of stacking faults is relatively low, explaining its good plasticity. When nickel is alloyed to austenitic steel it also increases the stacking fault energy of the iron matrix. The magnitude of the effect was found to be  $\sim 2.8$  mJ/m<sup>2</sup> per wt.% nickel added [45]. This value is larger than that for other alloying elements such as molybdenum ( $\sim 2.0$  mJ/m<sup>2</sup>), chromium ( $\sim 0.4$  mJ/m<sup>2</sup>) and manganese ( $\sim 0.75$  mJ/m<sup>2</sup>) per wt.% addition [45]. The level of stacking fault energy has an impact on the deformation characteristics of the material such as the work-hardening and softening behavior. Low SFE values, typically less than 45 mJ/m<sup>2</sup>, lead to widely dissociated dislocations whose movements are therefore confined to the slip planes, whereas localized cross-slip is extremely difficult. Higher SFE results in a lower barrier to dislocation motion due to the ability of cross slipping without splitting up into partial dislocations. The reduction of Peierls stress, in combination with the increase in dislocation mobility assisted by higher SFE (Figure 6) in nickel alloyed steels, is the metal-physical origin for improved toughness properties under impact loading (see Section 2.6) as well as better ductility in cold-forming processes.

The work-hardening rate is controlled by ease of cross-slip governed by the SFE, which in austenitic stainless steel is influenced by alloying elements [46]. Regarding carbon steels, the SFE and potential effects by nickel alloying are relevant to hot deformation in the austenite range and the behavior of potentially retained austenite phases in final condition. Strain hardening and softening processes take place alternately during hot rolling of the austenitic microstructure. Softening is caused either by recovery or recrystallization. The increase of the SFE by nickel alloying and the correspondingly improved dislocation mobility should promote recovery as softening mechanism during hot deformation. However, the overall recrystallization kinetics of the steel is not noticeably changed by nickel. Only the solute-drag effect caused by substitutional solutes delays the speed of the necessary grain boundary movement for a given recrystallization driving force. Retained austenite in carbon steel deforms by various secondary plasticity mechanisms, such as mechanical twinning ( $18 \lesssim \gamma \lesssim 45$  mJ·m<sup>-2</sup>) and martensite transformation ( $<18$  mJ·m<sup>-2</sup>) [47]. In that respect, the amount of nickel partitioned to the retained austenite might influence the mechanical properties of this phase.

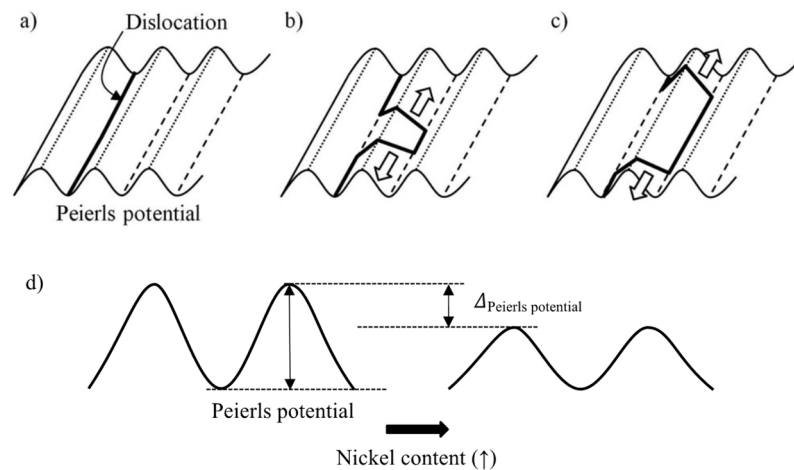


**Figure 6.** Kink pair nucleation and expansion mechanism moving a screw dislocation across the Peierls potential from one energy valley to the next. (a) Original position of screw dislocation aligned to a Peierls valley. (b) Activation of a kink pair partially crossing the Peierls peak. (c) Expansion of the kink pair under low stress. (d) Effect of nickel alloying lowering the Peierls potential and facilitating kink crossing.

### 2.5. Nickel Interaction with Copper

Copper alloyed steels are sensitive to cracking during hot forming operations, a phenomenon also known by the term “hot shortness” [48]. This phenomenon typically occurs at temperatures above 1000 °C due to copper enrichment at the steel surface below the iron oxide (FeO) layer [49]. When the copper enrichment reaches a level exceeding its solubility limit in iron, copper-rich phases precipitate at the interface between oxide scale and metal. The solubility of copper in austenite in the relevant temperature range is in the order of 8 wt.% [50]. The penetration of liquefied copper-rich phases along the austenite grain boundary cause liquid metal embrittlement (LME) and result in the disintegration of the steel under the simultaneous action of mechanical stress. Nickel alloying has two effects in this respect, alleviating or preventing this detrimental LME effect of copper. Firstly, nickel increases the solubility of copper in austenite [51], thus retarding the precipitation of copper-rich phases. Secondly, nickel, which also enriches at the interface between the oxide scale and metal surface, is completely miscible with copper in their binary alloy system. The solidus temperature increases nearly linearly from 1083 °C for pure copper to 1453 °C for pure nickel. Accordingly, the melting temperature of a 50%Cu–50%Ni alloy is at around 1250 °C. This temperature generally represents an upper limit for steel soaking before hot deformation is performed, usually at temperatures below 1200 °C. Hence, the simultaneous addition of nickel and copper in equal amounts successfully prevents hot shortness. More recent research has suggested that the addition of nickel in the ratio Ni:Cu = 1:2 might be sufficient for suppressing the hot shortness problem when copper is at residual levels originating, for instance, from recycling scrap used in electric arc furnace operations [52].

Regarding slab straightening after continuous casting, another hot ductility reducing effect of copper is related to the precipitation of fine copper sulfide or oxysulphide particles at austenite grain boundaries [53]. The increased solubility of Cu in austenite due to Ni alloying reduces the driving force for Cu precipitation, thus restoring the hot ductility for both straightening and hot rolling. Moreover, Ni appears to have a beneficial influence on the hot ductility of HSLA steels and also in the absence of Cu [53]. This effect has been related to the coarsening of micro-alloy carbonitride precipitates, which may be due to the enhancement of carbon activity by nickel alloying (see Section 2.2).

A subclass of HSLA steels employs copper precipitation for the production of high strength in addition to that which can be achieved by the more commonly used micro-alloy precipitation. The low carbon content in these steels, in combination with fine  $\epsilon$ -Cu particles precipitated during a thermal ageing process, impart a favorable combination of strength

and toughness to such steels [54]. In peak-aged condition, the coherent copper precipitates with bcc lattice structure generally have an average diameter of between 1 and 5 nm. The magnitude of precipitation strengthening is controlled by the number density of these particles and can reach several hundred MPa. Nickel alloying to such copper-based age hardening steels is advisable due to the priorly mentioned hot shortness problems. In addition, synergies between the two elements regarding the formation of nano-precipitates have been revealed in Cu–Ni alloyed steels. Zhang and Enomoto [55] have described the way in which the particle number density of a 1.5% Cu-alloyed steel almost doubled under the same treatment conditions when 3%Ni was co-alloyed. The higher particle count seems to be related to a significantly increased particle nucleation rate in the Cu–Ni steel. However, the particle size was only slightly larger under the same ageing conditions. The TTT curves describing the kinetics of Cu precipitation are clearly shifted towards shorter times by nickel alloying. Vaynman et al. [56] exploited this Cu–Ni precipitation synergy for the design of a 965 MPa (140 ksi) steel by alloying 1.3%Cu and 2.7%Ni to a very low carbon base chemistry. The detailed analysis of the precipitates using atom probe tomography (APT) revealed the segregation of Ni, Al, and Mn to the precipitate/ferrite matrix interfaces of the Cu-rich precipitates after longer ageing time. A more recent work by Jiao et al. [57] has revealed substantial precipitation strengthening in ferritic steel by using 2%Cu in combination with 0.75%Ni. While the copper-only alloyed steel achieved a precipitate strengthening effect of 132 MPa, the addition of nickel increased the magnitude of this effect to 437 MPa. It has been argued that the inclusion of Ni atoms in a Cu-rich nucleus decreases the strain energy for nucleation. Furthermore, segregation of Ni atoms to the particle/matrix interface also decreases the interfacial energy.

## 2.6. Nickel Effect on Toughness

One of the most prominent effects of nickel in carbon steels is its improvement of toughness properties. A transitional behavior from ductile behavior with high upper-shelf energy (USE) to brittle failure with lower-shelf energy (LSE) is observed in steel with a bcc lattice structure when characterizing toughness by Charpy impact testing (Figure 7a). The temperature at which the fracture surface has an equal share of ductile and brittle appearance is typically defined as the ductile-to-brittle transition temperature (DBTT). The DBTT of the selected bcc steel must be lower than the lowest encountered operating temperature in a technical application.

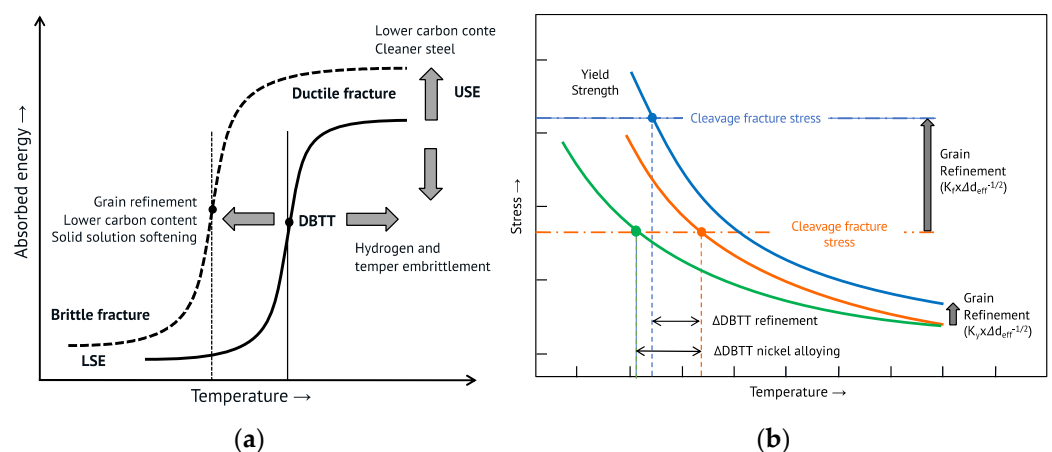


**Figure 7.** (a) Ductile-to-brittle transition behavior of bcc steel and influencing factors; (b) principles of lowering DBTT by grain refinement and solid solution softening (nickel alloying).

The evolution of steel development over the recent decades has focused on two major toughness-optimizing criteria in addition to generally lowering impurity levels and avoiding inclusions (Figure 7a). The reduction of the carbon content results in an increase of USE and a significant decrease of DBTT [58] while weldability is improved simultaneously.

Grain refinement raises yield strength and also strongly decreases DBTT (Figure 7b). Thus, grain refinement is the only strengthening mechanism that is also beneficial for toughness. The combination of low-carbon alloy design with maximized grain refinement achieved by thermomechanical rolling and accelerated cooling has led to high strength steels that behave as fully ductile at temperatures as low as  $-60\text{ }^{\circ}\text{C}$ , i.e., DBTT is at around  $-80\text{ }^{\circ}\text{C}$  [59,60]. However, this approach is beginning to reach its limits, wherein either applications require a very low DBTT, a low carbon content is not applicable, or product processing does not allow the application of substantial thermomechanical treatment for producing grain refinement.

Simplistically, the transition from ductile to intragranular (cleavage) fracture occurs when the effective yield strength at a certain low temperature exceeds the cleavage fracture stress (Figure 7b). Both properties depend on grain size according to Hall–Petch type relationships as outlined in more detail by Morris [61]. However, the Hall–Petch coefficient of the fracture stress ( $K_f$ ), although dependent on the phase constitution of bcc steel (i.e., the size and distribution of carbide phases), is always larger than that of yield strength ( $K_y$ ) [62]. Yield strength shows a significant increase with decreasing temperature while the fracture stress experiences only a small change, mostly related to the temperature dependence of the elastic modulus. Due to the effects of solute nickel on the mobility of dislocations and therefore on the low temperature plasticity outlined in Section 2.4, solute softening can substantially lower DBTT in nickel alloyed steels irrespective of grain refinement. As the Ni content is increased, the resolved shear stress on the most favorably oriented slip system approaches the cleavage stress along the  $\langle 100 \rangle$  direction, and there is an increasing likelihood the crystal will shear before cleaving [29]. Nickel additionally increases the effective surface energy for cleavage fracture, thus contributing to a higher cleavage fracture stress according to Gerberich et al. [63]. The combination of both effects, namely reduced effective yield stress and increased cleavage fracture stress, results in a decreasing DBTT with nickel alloying from  $-32\text{ }^{\circ}\text{C}$  in the unalloyed reference iron (polygonal ferritic) to  $-100\text{ }^{\circ}\text{C}$  for 4 at.% Ni. Such nickel alloyed ferritic steels can compete with the best TMCP-rolled fine-grained low-carbon steels. As mentioned in Section 2.4, other alloying elements such as Mn, Cu, Si, or Al also provoke a solid solution softening effect at low temperature that could be principally used for DBTT improvement. However, contrary to nickel these alloys increase DBTT after an initial improvement due to competing effects that promote transgranular or even intergranular fractures at higher alloy additions [64,65].

Extremely low DBTT is required for steels used in cryogenic applications. As early as the early 1960's so-called "9Ni steel" had been established for cryogenic applications as a suitable alternative to austenitic steels. In 1964, Jesper and Achterlik [4] reported on the mechanical properties of cryogenic steel grades with nickel contents between 1.5 and 13 wt.%, covering the operating temperature range from  $-50$  to  $-200\text{ }^{\circ}\text{C}$ . These steels are typically produced by quenching and tempering (Q&T) treatment [4]. In addition to the mechanism by which solid solution softening accounts mainly for the improvement of low temperature toughness, the Q&T treatment results in a very fine grain structure and the formation of retained austenite islands. Nickel partitioning stabilizes a small fraction of retained austenite during tempering at temperatures in the two-phase region between the  $A_{c1}$  and  $A_{c3}$  temperatures (Figure 1c). An optimized retained austenite content results in exceptionally high toughness at temperatures below  $-100\text{ }^{\circ}\text{C}$ . Figure 8 exemplarily demonstrates the influence of the retained austenite on low-temperature toughness for a steel containing approximately 9 wt.% Ni [65].

The austenite phase fraction and the impact energy at  $-196\text{ }^{\circ}\text{C}$  behave congruently in the function of the tempering temperature of the steel. It should be noted that the initial reversed austenite is metastable and partially transforms into martensite when cooling to cryogenic temperature. Morris et al. [29] have pointed out that the toughness enhancing effect of retained austenite is not caused by "transformation toughening". Accordingly, the crystallographic variant forming upon transformation under load is that which best relaxes the local stress. It decomposes the martensite packet by introducing features of different crystallographic orientation with the effect of inhibiting cleavage fracture. For

an optimum exploitation of this mechanism, the precipitated austenite must be thermally stable and densely distributed through the microstructure. For that purpose, a relatively low tempering temperature close to the  $A_{C1}$  line is preferable.

#### Steel grade X8Ni9 (1.5662)

Alloy	C	Si	Mn	Cr	Ni	Cu
Wt.%	0.05	0.29	0.25	0.04	9.1	0.04

Condition:  
Quenched & tempered

Requirements:  
585 MPa minimum yield strength at room temperature  
70 J minimum required Charpy toughness at  $-196\text{ }^{\circ}\text{C}$

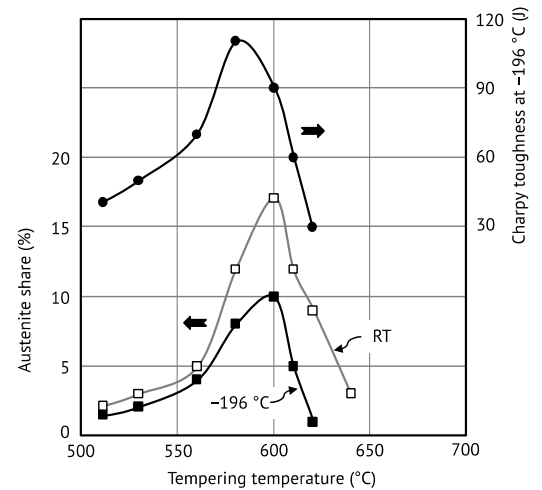


**Figure 8.** Correlation of Charpy toughness and retained austenite volume fraction at  $-196\text{ }^{\circ}\text{C}$  in a cryogenic steel alloyed with 9 wt.% Ni.

Empirical data of the Charpy toughness measured by notched bar impact testing can be closely correlated with the fracture toughness obtained by fracture mechanics testing. Thereby, the temperature for achieving a  $100\text{ MPa}\cdot\text{m}^{1/2}$  fracture toughness is related to the Charpy 27 J transition temperature as per [66,67]:

$$T_{KIC = 100} = T_{27} - 18\text{ }^{\circ}\text{C}. \quad (3)$$

Since nickel alloying reduces the  $T_{27}$  temperature, the fracture toughness is correspondingly improved at lower temperature.

#### 2.7. Nickel Effect on Environmentally Assisted Cracking (EAC)

Hydrogen has the highest diffusivity of all interstitial elements in the bcc iron lattice and interacts with defects and different types of hydrogen traps. The local accumulation of hydrogen at interfaces and defects causes various types of hydrogen embrittlement (HE) as well as hydrogen-induced cracking (HIC) or stress corrosion cracking (SCC) depending on the hydrogen concentration [68]. This problem is highly relevant to medium-strength HSLA steels continuously operating in contact with sour media and also typically to ultra-high strength steels even when occasionally undergoing hydrogen pick-up. Hydrogen is usually introduced into the iron lattice by adsorption of atomic hydrogen ( $H_{ad}$ ) as the result of a chemical reaction at the steel surface, providing dissolved hydrogen ( $H_{dis}$ ) in the bulk steel as schematically shown in Figure 9a. ISO standard 15156-2 [69] defines four severity regions regarding the risk for HIC and SCC depending on the pH value and on the  $H_2S$  partial pressure in the surrounding medium (Figure 9b). Currently, most low-alloyed carbon steels are accepted for service under any  $H_2S$  condition if they contain less than 1 wt.% nickel (max. limit of ISO 15156) and the hardness in the area exposed to the corrosive medium is kept below 250HV (22HRC). A detailed analysis of nickel's effect on SCC has been performed by Kappes et al. [70], who concluded that limiting the nickel content to 1.0 wt.% constrains materials selection and imposes serious economic and operational penalties for both high pressure and high temperature as well as arctic oil and gas operations.

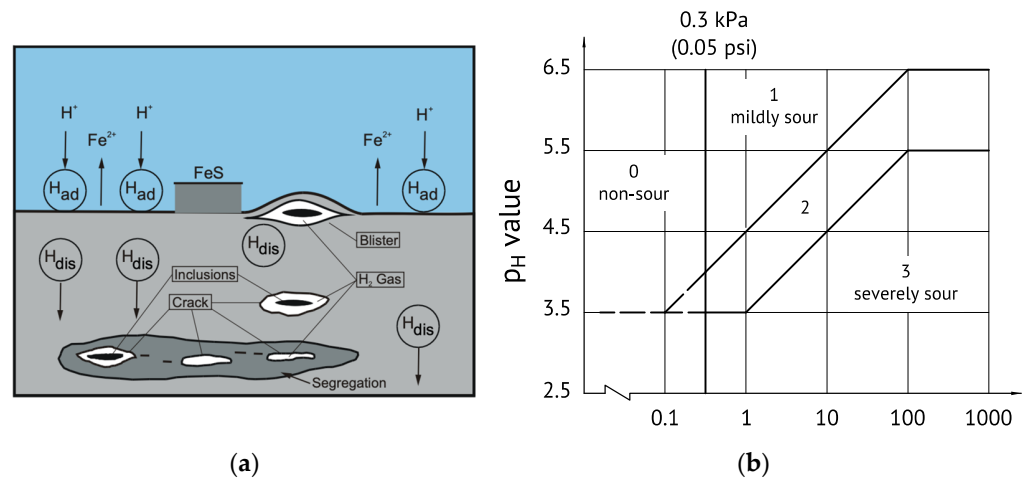


**Figure 9.** (a) Principle of hydrogen generation by a corrosive reaction at the steel surface and typical damage features by absorbed hydrogen in the steel; (b) definition of environmentally assisted cracking (EAC) severity regions according to ISO standard 15156-2.

Metallurgical development in the 1980's towards the production of sour-resistant line pipe steels with a yield strength in the range of 450–550 MPa, indicated that Cr, Cu and Ni alloying is effective in reducing the steel's corrosion rate in aggressive media and accordingly lowers the hydrogen pick-up from the surface into the steel [71]. While in a mildly sour environment (pH = 5.2) the corrosion inhibiting effect of these alloying elements is rather comparable, nickel alloying becomes clearly the most effective alloy in more aggressive environments at the lower pH value of 4.0 (Figure 10).

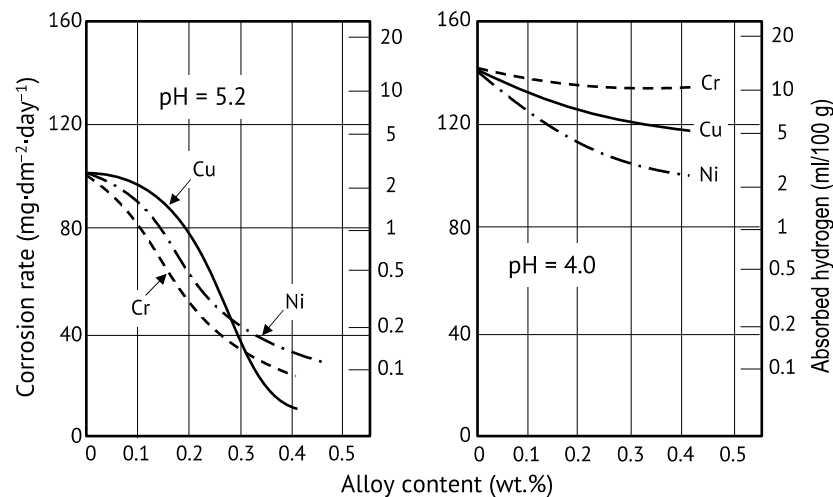


**Figure 10.** Influence of Ni, Cu, Cr alloy content on the corrosion rate and hydrogen absorption of low-carbon line pipe steel exposed to a sour  $H_2S$  containing environment (courtesy of K. Hulka, Niobium Products Company, Düsseldorf, Germany—based on data from [71]).

From a more extensive review on nickel effects influencing the environmental assisted cracking (EAC) behavior of carbon steels by Jarvis and Bulloch [68] it can be taken that improvements are related to (1) reduced overall corrosion rates and (2) decreased lattice diffusion of hydrogen. Since nickel promotes the formation of a protective layer by local enrichment at the steel surface, the effects of anodic dissolution will be reduced as the nickel content increases. The anodic dissolution of iron results in a corrosive weight loss. The corrosion rates shown in Figure 10 suggest that this inhibiting effect becomes saturating above an alloy content of 0.4 wt.% Ni [71]. Experiments on a medium carbon ultra-high strength steel (1500 MPa) immersed for 100 h in a pH 3.5 Walpole solution indicated the

same trend [72]. The corrosion rate clearly decreased for Ni addition of up to 0.5 wt.% while raising the Ni content to 1.0 wt.% showed only marginal further improvement. The open-circuit potential value obtained from polarization measurements, however, increased consistently with the nickel content. This occurred with a decreasing corrosion pit depth with increasing Ni content, reducing stress concentration. Nowadays, developments for automotive steels have been targeting a strength level of 2000 MPa. Such steels are very sensitive to hydrogen embrittlement and alloying strategies are therefore being developed to cope with that problem [73]. In this regard, the effect of nickel alloying to medium-carbon steel (C content: 0.4–0.5 wt.%) was also investigated for additions in the range of 0.1 to 1.2 wt.% [74]. Auger electron spectroscopy confirmed the presence of an approximately 4-nm thin nickel-enriched layer at the metal surface below the iron oxide scale. Immersion of these steels in a neutral aqueous environment of 3.5% NaCl indicated that the weight loss by corrosion linearly decreased with increasing nickel content up to 1.2 wt.% in this moderately aggressive medium. However, the reduced corrosive weight loss and the lower total uptake of hydrogen into the steel did not necessarily materialize in a better resistance against hydrogen embrittlement.

The observed incongruity of hydrogen embrittlement behavior in the function of nickel alloy addition relates to adverse microstructural effects competing with the beneficial functionality of nickel enrichment at the metal surface. Such microstructural features are the result of the alloy composition and heat treatment. It has been shown that by nickel's effect of lowering the  $A_{c1}$  temperature, dissolution of cementite might not be completed during the re-austenitizing phase [75]. Initially formed Ni-rich austenite films obstruct the out-diffusion of carbon from dissolving cementite so that incompletely dissolved particles can be retained in the final product. Cementite particles in a corrosive environment act as a localized anode, especially when they are concentrated in the near-surface (Ni-enriched) layer [75]. As outlined above, nickel alloying in combination with suitable heat treatment can also promote the formation of retained austenite. Hydrogen has a high solubility in austenite, while its diffusivity is low. Hence retained austenite islands in a ferritic microstructure act as an irreversible hydrogen trap, which in first place might be considered beneficial. However, when metastable retained austenite transforms into martensite triggered by plastic deformation, for instance at the tip of a proceeding crack, trapped hydrogen becomes highly diffusible in an area that simultaneously experiences high local dilatation stresses [70]. Under such circumstances cracking might even be accelerated. Accordingly, retained austenite cannot be considered beneficial to improve SCC resistance [76].

The interstitial lattice sites around substitutional solute atoms act as a reversible hydrogen trapping site. With increasing solute content, the hydrogen permeability and diffusivity should hence decrease. The interaction energy between hydrogen and the solute atom is expectedly related to the misfit parameter. Hagi [27] has described the effect of several substitutional alloying elements on the diffusion coefficient of hydrogen in pure  $\alpha$ -iron. The chosen approach excluded any implications related to carbon containing phases and also avoided other potential trapping effects. Nickel alloying in the range of up to 5 at.% significantly reduced the hydrogen diffusivity from approximately  $10^{-8}$  m<sup>2</sup>/s (Ni-free) to  $5 \times 10^{-9}$  m<sup>2</sup>/s (5 at.% Ni) at ambient temperature. Thereby the diffusivity reducing effect of nickel was larger than that of chromium, with a similar misfit parameter. It also had a similar misfit parameter as aluminum, inducing a much higher lattice misfit. The interpretation of this apparent inconsistency is that hydrogen diffusivity is not only influenced by elastic interaction (misfit) but also by chemical (electronic) interaction between the alloy atom and hydrogen. Experimental results from Husby et al. [14] on ferritic-pearlitic steels (carbon content: 0.17 wt.%) with different nickel contents in the range of 0 to 3 wt.% showed the same trend regarding the effective hydrogen diffusion coefficient. These investigated steels had nearly the same grain size, but the pearlite fraction increased with the nickel content, likely additionally influencing the hydrogen diffusivity.

The relevance of grain size on the susceptibility of SA517 Grade F steel to hydrogen environment embrittlement in a 45 MPa gaseous hydrogen atmosphere has been demonstrated by Takasawa et al. [77] using two Ni alloy levels (1 and 2 wt.%). The notch fracture stress under pressurized hydrogen conditions increased with the ASTM grain size number (i.e., finer grain size) while the influence of the nickel content appeared to be marginal. The amount of diffusible hydrogen picked up by the steel during tensile testing was higher the larger the grain size. Simultaneously, the hydrogen concentration per unit grain boundary area increases with larger grain sizes, which is the main reason for reduced fracture stress. At first sight, the nickel content has thusly no influence on these results. However, the decrease in  $A_{c3}$  temperature with increasing nickel content (see Figure 1b) allows for re-austenitizing of the steel at lower temperatures. This results in a limitation of austenite grain growth. In that sense, nickel alloying can indirectly improve hydrogen embrittlement resistance.

### 2.8. Influence of Nickel on Fatigue Behavior

Most constructions are subjected to cyclic loading at stress levels below yield strength. Under these conditions, the microstructure experiences fatigue reducing the bearable strength level. Failure of components subjected to cyclic loading under different loading scenarios (pulsating, alternating, etc.) consists of two stages: crack initiation and crack growth until the fracture toughness is reached. This particularly applies to the low-cycle fatigue domain. Depending on the applied stress, the Wöhler curve indicates the number of load cycles that can be endured until the occurrence of fatigue fracture. The Wöhler curve is divided into the domains of low-cycle fatigue and fatigue endurance. Nickel has a positive effect on the improvement of fatigue strength of structural steels by enhancing the fracture toughness, especially at low temperatures, as shown in Section 2.6 and according to Equation (3). Fracture toughness determines the crack growth rate  $da/dN$  as a function of the stress intensity factor  $\Delta K$  ahead of the crack according to the well-established Paris–Erdogan crack propagation law:

$$da/dN = C \cdot \Delta K^m \quad (4)$$

The constants  $C$  and  $m$  can be determined from a log–log plot. Tobler and Cheng [78] defined two regions:

- (1) In a low-toughness region  $m$  increases as  $K_{1c}$  decreases; temperature, Young’s modulus and yield strength influence the fatigue performance as well.
- (2) In a high-toughness region  $m$  remains constant and independent of  $K_{1c}$ .

Nickel alloyed ferritic steels were shown to have a constant  $m$ -value in the range of 2 to 4 at ambient temperature, irrespective of the nickel content [78]. When testing fatigue crack growth at 76 K, however, the  $m$ -value exhibited a strong linear correlation with the nickel content between 0 and 5 wt.% whereas steels with nickel additions above 5 wt.% behaved according to the high-toughness region. Park et al. [79] recently confirmed this behavior for various Q&T steels containing between 3.5 and 9 wt.% Ni. They point out that, especially at low service temperatures, the crack-growth rate for a given stress intensity level is lowered by the addition of Ni. However, they remark that the  $K_{1c}$  parameter does not accurately reflect the plastic deformation and related strain hardening occurring in the neighborhood of the crack tip. Therefore, the transition temperature between toughness regions (1) and (2) may be predicted inaccurately by using  $K_{1c}$ . Alternatively, a correlation between CTOD and  $m$ -value was suggested for determining the transition temperature from ductile to brittle fatigue fracture.

### 2.9. Influence of Nickel on Welding Behavior

Nickel is the only alloying element that improves strength and toughness properties simultaneously without having a significantly negative effect on weldability. This is

reflected in the various empirical definitions of the carbon equivalent (CE) used for judging the weldability of steels, of which the most important are:

$$CE(IIW) = C + Mn/6 + (Cu + Ni)/15 + (Cr + Mo + V)/5 \quad (5)$$

$$CET = C + (Mn + Mo)/10 + (Cr + Cu)/20 + Ni/40 \quad (6)$$

$$P_{cm} = C + Si/30 + (Mn + Cu + Cr)/20 + Ni/60 + Mo/15 + V/10 + 5 \cdot B \quad (7)$$

The multiplying factor of nickel is smaller than that of other common alloying elements such as Cr, Mo, Si, V, and Mn in all three CE definitions. The nickel alloy addition to weldable structural steels is limited by commonly applied standards for structural steels (EN-10025-3/-4: 0.8 wt.%, EN-10225: 0.7 wt.%, Norsok: 1.0 wt.%), i.e., its maximum contribution to these CE definitions (Equations (5)–(7)) is 0.067, 0.025 and 0.017, respectively.

The toughness-increasing effect related to nickel alloying discussed in Section 2.6 is also reflected in the properties of welded joints. This holds for the coarse-grained heat affected zone (CGHAZ) [80,81] as well as for the weld metal [82–84]. Nickel retards the nucleation and growth kinetics of grain boundary ferrite, refines the microstructure, and increases the share of acicular ferrite at the expense of grain boundary ferrite (Figure 2b). Huang et al. [81] have demonstrated this effect in low-carbon steels containing up to 0.5 wt.% Ni. They also noticed a reduced fraction of the detrimental MA phase. Nickel alloying markedly increased the CGHAZ toughness at  $-20\text{ }^{\circ}\text{C}$  for low and high heat-input welding conditions, with ductile fracture appearance in both cases. You et al. [80] investigated the influence of higher nickel additions (0.8 and 3.7 wt.%) on the CGHAZ microstructure. For the selected weld cycle representing a heat input of  $6\text{ kJ/cm}$ , the applied NbTi micro-alloy concept could not prevent substantial austenite coarsening at a peak metal temperature of  $1300\text{ }^{\circ}\text{C}$ . However, CGHAZ toughness at  $-20\text{ }^{\circ}\text{C}$  was maintained at a high level. It appeared that the benefit of nickel alloying is not related to austenite refinement but rather to an optimization of microstructural features developing within the rather coarse prior austenite grains upon transformation. A detailed microstructural analysis led to the conclusion that with increasing nickel content the microstructure changes from a mix of acicular ferrite plus lower bainite to pure lower bainite with a reduced fraction of carbon-rich islands (retained austenite and MA). In that sense, a higher nickel content, lowering the transformation temperature, makes the transformation more complete and uniform, thus suppressing carbon partitioning as a mechanism for the formation of unwanted hard phases. Furthermore, a higher nickel content changes the configuration of the Bain groups in the crystallographic packet within the prior austenite grain while the density of high-angle boundaries remains almost the same [80].

Property demands regarding weld metal also focus on a combination of high strength and good toughness. The weld metal representing a solidification microstructure has limited possibilities for property optimization except by alloying. Often the alloy content needs to be substantially raised for matching weld metal strength to the base metal. The initially columnar austenitic microstructure of the weld metal decomposes into grain boundary ferrite (GBF), ferrite side plates (FSP), acicular ferrite (AF) and, in certain circumstances, MA constituents. AF microstructure can be considered favorable for strength and toughness while GBF and FSP are detrimental. Both Mn and Ni affect the microstructure in a similar way by depressing the transformation temperature, thus, preventing GBF and FSP formation in favor of AF. Accordingly, welding consumables for demanding tasks often employ increased Mn and Ni contents. Zhang and Farrar [84] investigated suitable combinations of both alloying elements. It was found that Mn additions in the range of 0.7 to 1.5 wt.% and nickel contents between 1.0 and 3.5 wt.% deliver the best weld metal toughness. Regarding low temperature toughness, the functionality of nickel is superior to that of manganese for reasons outlined in Section 2.6. The addition of nickel to the weld metal effectively promotes the formation of acicular ferrite while significantly reducing the amount of grain boundary ferrite, both at the higher and lower manganese levels [84]. A nickel content over 5 wt.% produces larger amounts of martensite and coalesced bainite.

Martensite can form also in interdendritic regions as a consequence of significant nickel and manganese segregation in weld metals containing 7–9 wt.% Ni and 2 wt.% Mn [85]. A systematic investigation of Ni–Mn alloy combinations in ultra-low carbon (<0.02 wt.%) weld metals by Kang et al. [6] arrived at similar conclusions. It is favorable to decorate prior columnar austenite grain boundaries with grain boundary ferrite to prevent the risk of intergranular fracture for the reasons explained in Section 2.1 (see also Figure 1c). In that sense manganese should range between 0.5 and 1.0 wt.% while the nickel content is recommended to be in the range of 4 to 5 wt.%. Alloy combinations within those ranges have achieved high weld metal toughness even at temperatures as low as  $-80\text{ }^{\circ}\text{C}$ .

### 3. Application of Nickel Alloying in Carbon Steel Strip and Plate Products

In the following sections some representative examples will demonstrate the implementation of nickel alloying and its effects in two classes of products. The first example addresses HSLA steels with nickel additions below 1 wt.% under TMCP processing conditions without heat treatment. The second example considers higher nickel alloying up to 9 wt.% in heat treated cryogenic steels. Both case studies are based on the extensive experience of the current authors in designing and producing respective nickel alloyed steels.

#### 3.1. Nickel Alloying in HSLA Steels for Structural and Line Pipe Applications

Nickel alloying is relevant to the production of HSLA steels for structural as well as pipe applications. This is related to its prominent effects as discussed in the foregoing sections. To briefly summarize, nickel is the only element shown to improve notch toughness (DWTT, CTOD and Charpy values) when all other relevant factors (e.g., grain size and precipitation hardening) are fixed. It can be used to mitigate the harmful effect of residual or intentionally added copper on hot shortness. Nickel is beneficial for reducing hydrogen charging rates in sour ( $\text{H}_2\text{S}$ ) service and is often used in combination with copper for that purpose. In structural steels S235–S460 (normalized condition) with ferritic-pearlitic microstructure, the addition of 1% Ni results in a moderate yield strength increase of around 50 MPa. In combination with other alloying elements, nickel promotes the formation of strong microstructures allowing the production of ultra-high strength steels with good low-temperature toughness.

Different rolling processes, such as conventional, normalizing, and thermo-mechanical rolling (TMCP), can be used to produce HSLA steels. TMCP steels comprise high yield strength, good toughness, and excellent weldability in combination. Rolling under TMCP conditions requires a sufficiently high reduction ratio below the temperature of non-recrystallization to obtain pronounced austenite pancaking, resulting in the desired grain refinement upon transformation. Initial rough rolling, on the contrary, aims for multiple full recrystallization throughout the slab thickness providing a homogeneous and equiaxed austenite grain structure to the non-recrystallizing finish rolling process. The respective reduction schedules of finish and rough rolling must be matched to the available slab thickness and final product gauge. In particular, the production of heavy-gauged plates often requires compromises to be made when designing a rolling schedule, which typically affects the roughing stage and causes low deformation in the slab center. This can lead to insufficient recrystallization and partial coarsening of austenite grains particularly in the mid-section of the product. Such a microstructural inhomogeneity cannot be removed by subsequent non-recrystallizing rolling, with the consequence of deteriorated toughness properties in the plate center zone. The situation may be additionally aggravated because this area is also a potential segregation zone and experiences lower cooling rates after finish rolling. Therefore, mid-thickness strength and toughness are often relatively poor under these circumstances. When specifications demand verification of mid-thickness properties, nickel alloying is typically the only possible solution. Figure 11a indicates that the specific effect per wt.% Ni added is nearly unaffected by the cooling rate or degree of austenite deformation.

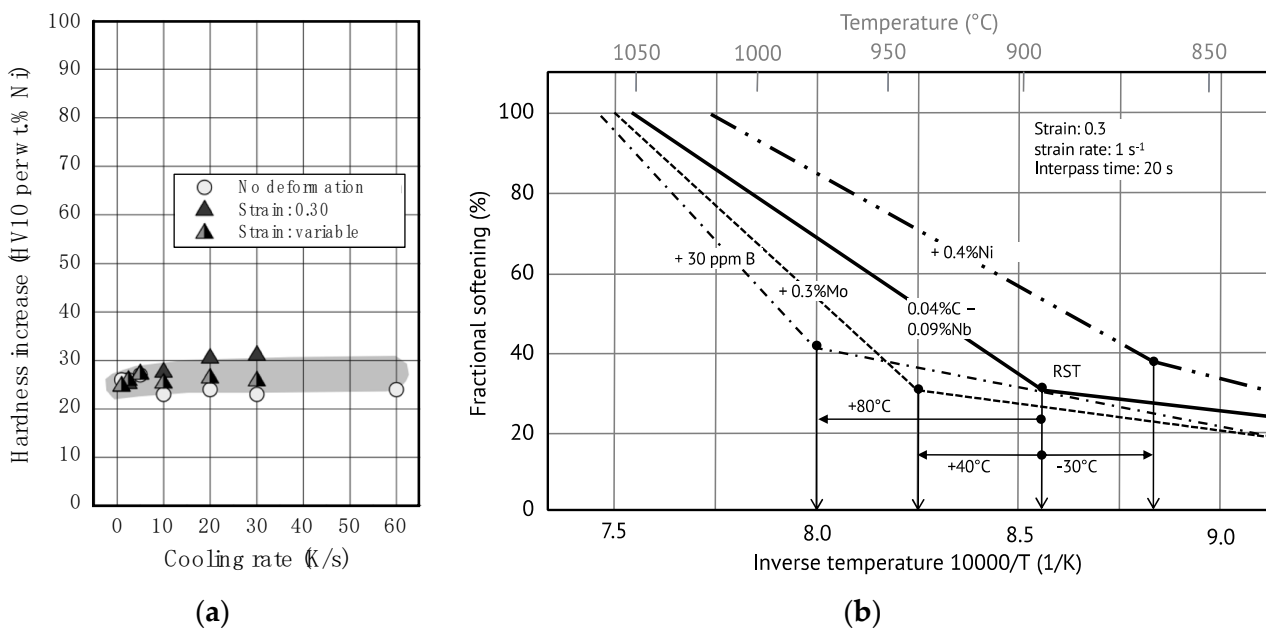


**Figure 11.** (a) Rated hardness increase by nickel alloying in function of cooling rate and austenite deformation in low-carbon steel. (b) Fractional softening behavior of 0.04 wt.% C 0.09 wt.% Nb steel during simulated austenite deformation (measure by hot torsion testing) and influence of additional alloying elements Mo and B (RST: recrystallization-stop temperature).

More recently, an advanced HSLA concept relying on extra-low carbon content in combination with higher niobium micro-alloy additions have become popular for use in heavy plate and strip products [86,87]. The base alloy has an inherently high recrystallization-stop temperature (RST), as can be noticed from the fractional softening behavior shown in Figure 11b. Even at temperatures of 1000 °C does recrystallization become measurably delayed, allowing performance of TMCP rolling higher than in traditional HSLA steel concepts. When adding other alloying elements, such as molybdenum or boron, to this base concept, the RST further increases by 40–80 °C. While a high RST is advantageous regarding TMCP rolling, delayed recrystallization at temperatures above 1000 °C is problematic as it interferes with rough rolling, especially when using low slab discharge temperatures. Nickel alloying has been found to have an opposite effect, by lowering RST and promoting softening in the temperature range of rough rolling [88]. Therefore, nickel allows the mitigation of the softening behavior in complex alloys, and thus facilitates homogenization of the microstructure during rough rolling.

Depending on the niobium content, these steels show different responses to the cooling conditions after TMCP rolling (Figure 12). For high cooling rates (>30 K/s) and low cooling-stop temperatures (<500 °C) not much hardness difference is observed in the final product. The niobium micro-alloyed steels have a better hardenability due to the transformation retarding effect of solute niobium (Figure 12a). Low cooling rates and high cooling-stop temperatures reveal the strong influence of niobium. A higher solute Nb alloy content promotes strengthening by transformation delay and also offers more precipitation strengthening after transformation (Figure 12b). At low cooling-stop temperature precipitation will be effectively suppressed. In plate rolling, both conditions can be present, depending on whether the position is closer to the surface or closer to the centerline. This discrepancy becomes more pronounced as the plate gauge increases.

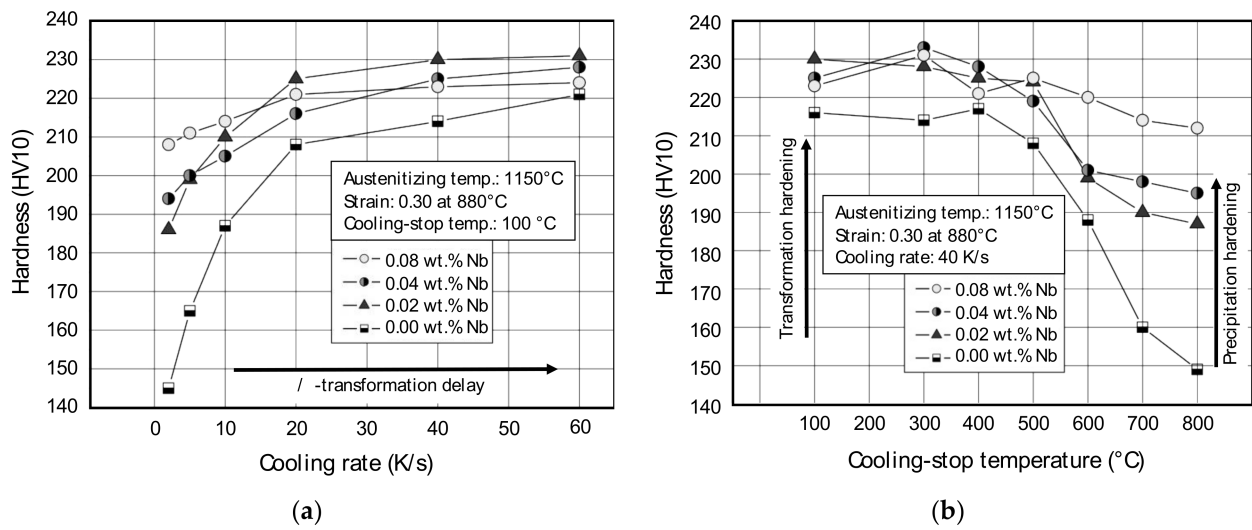


**Figure 12.** (a) Effect of cooling rate and (b) cooling-stop temperature on the hardness of TMCP rolled 0.03 wt.% C–1.5 wt.% Mn steel with varying Nb micro-alloy content.

Nickel alloying, however, can balance out these differences by enhancing the hardenability in the center region in synergy with solute niobium. Naturally, a thicker gauge will require a higher nickel addition to compensate the larger difference. Plate-mill results shown in Figure 13a demonstrate a remarkable consistency of strength properties for a wide range of processing parameters as well as plate gauges using a higher Ni content above a 40 mm gauge. All plate gauges fulfill the strength requirements of API grades X65 and X70. Toughness measurements on 28-mm thick plates reveal a very low transition temperature of around  $-120$  °C (Figure 13b), which is the combined result of extra-low carbon content, severe grain refinement and nickel alloying. Besides mainstream pipe and structural applications [86,89], this steel concept is well-suited for sour gas pipes or for backing plates used in clad pipe production [90]. Upgrading this base alloy concept by additionally using combinations of molybdenum, chromium, copper, or boron, and applying a TMCP and accelerated cooling processing route allows the production of steel grades in the range of 500 to over 800 MPa yield strength while maintaining excellent toughness properties [91].

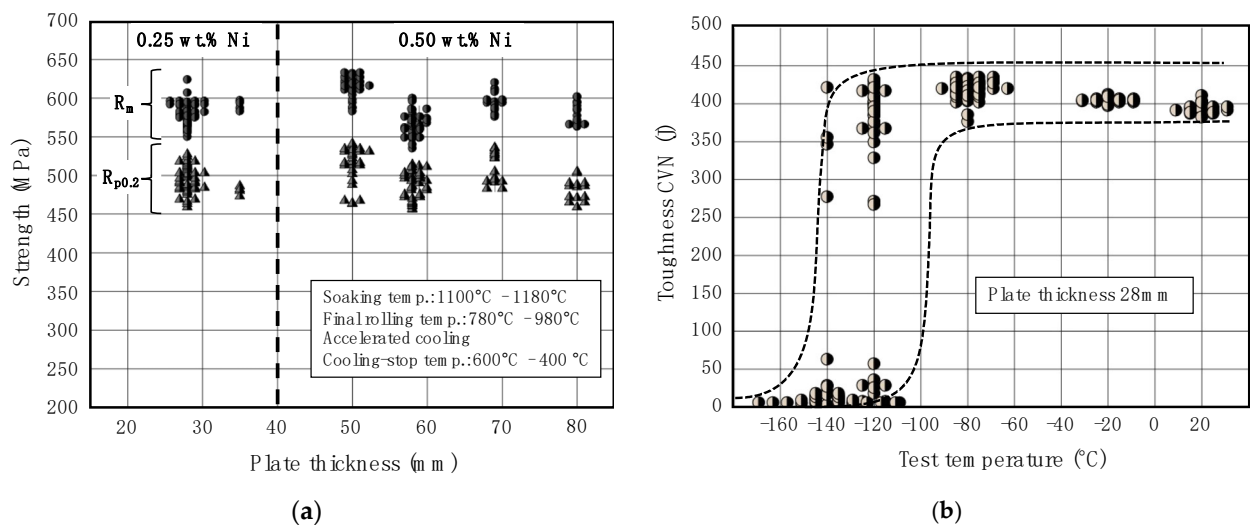


**Figure 13.** (a) Strength properties obtained by plate-mill trials with a 0.03 wt.% C–1.5 wt.% Mn–0.08 wt.% Nb steel and variable nickel alloying adapted to plate gauge. (b) Charpy V-notch toughness transition behavior for a respective steel plate with 28-mm thickness (all data taken at 1/4 thickness position in longitudinal and transverse direction).

### 3.2. Nickel Alloying in Cryogenic Steels for Liquefied Gas Technology

Cryogenic steels are mainly used for manufacturing equipment serving the storage as well as the production and transportation of hydrocarbons. Liquefaction of such gases reduces their volume by up to 600 times, thus requiring less space for storage and transport. This technology is gaining significant importance due to a switch from pipeline delivered natural gas towards more flexible LNG supplies. Furthermore, future green energy technologies will use liquefied gases as storage and transport medium. Figure 14 shows the boiling temperatures of various industrial gases and the corresponding nickel content to be used in the steel. As the boiling temperature of the gas decreases, the Ni-content of the steels increases up to a maximum of approximately 9 wt.%.

Short name / Material no.	Nickel content (wt.%)	Min. yield strength at room temp. (MPa)	Impact toughness *)		Gas technology / Boiling temperature (°C)												
			Test temp. (°C)	Min. energy (J)	Butane	Propane	Propene	Carbon dioxide	Ethane	Ethylene	Methane	Oxygen	Argon	Nitrogen	Hydrogen	Helium	
					-0	-42	-47	-78	-89	-104	-161	-183	-186	-193	-253	-269	
11MnNi5-3 1.6212	0.3–0.8	285	-60	40													
13MnNi6-3 1.6217	0.3–0.85	355	-60	40													
12Ni14 1.5637	3.25–3.75	355	-100	40													
X12Ni5 1.5680	4.75–5.25	390	-120	40													
X8Ni9 1.5662	8.5–10	585	-196	70													

\*) Charpy V-notch sample, longitudinal test direction, average value of 3 individual tests

**Figure 14.** Properties and application ranges of nickel-alloyed cryogenic steels for liquefied gas technology.

The composition and required mechanical properties of cryogenic steels are usually specified in accordance with the DIN EN 10028-4 standard [92]. In particular, steel grades X7Ni9 or X8Ni9, containing approximately 9 wt.% Ni, have equivalent grades according to ASTM/ASME, which are frequently requested for tanks projects outside Europe. Nickel-alloyed steels, especially those with 9 wt.% Ni content, meet high requirements concerning toughness at low temperatures and simultaneously high strength. The Ni addition is the decisive parameter for achieving sufficient low-temperature toughness (Figure 15). It is clear that only for Ni contents above 3 wt.% is there any prospect of safely achieving T27 transition temperatures lower than  $-160$  °C. On the less-demanding end of the range, steel grade 13MnNi6-3 is commonly used for the construction of liquefied petroleum gas (LPG) tanks with operating temperatures as low as  $-50$  °C. The reduced carbon content in conjunction with production by normalizing treatment results in a very high toughness level and improved cold workability as compared to conventional structural steels. A minimum yield strength of 355 MPa allows the combination of high operational safety with weight-optimized design. More widely used is steel grade X12Ni5 with about 5 wt.% Ni, especially for constructing gas tanks for liquid ethane transport as well as deep-submergible vessels [93]. This steel is usually supplied in water-quenched and tempered condition. Common test temperatures for toughness verification of this grade are  $-110$  to  $-130$  °C, depending on the plate thickness [92]. Steel grade X7Ni9/X8Ni9, as well as its ASTM equivalent grade A553, has the highest nickel content of 9 wt.% and is also mainly produced by water quenching and tempering. It is typically used for the construction of LNG tanks with operating temperatures of around  $-160$  °C. Due to its high minimum yield strength of 600 MPa, the steel is excellently suited for lightweight structures using low

container wall gauges. The recent trend towards increasingly larger LNG-tank capacities (>200,000 m<sup>3</sup>), however, requires plate gauges up to 50 mm. Molybdenum alloying has been successfully used to achieve the mechanical properties in such heavy gauged 9%Ni steels [94]. It should be mentioned that steel grade 12Ni14, with about 3.5 wt.% Ni, is also technically and economically significant and can be used, e.g., for the transport and storage of liquefied carbon dioxide or ethane. Under the condition of high cleanliness and low phosphorus and sulfur residuals, a good notched-bar impact toughness of above 27 J can be achieved even at a test temperature of −120 °C. The steel is usually supplied in normalized condition while water quenching and tempering results in slightly more favorable properties.

Base alloy	C	Si	Mn	P	S	Al
Wt.%	~0.10	~0.30	~1.0	~0.02	~0.009	~0.035

30 mm plate thickness  
Water quenched & tempered

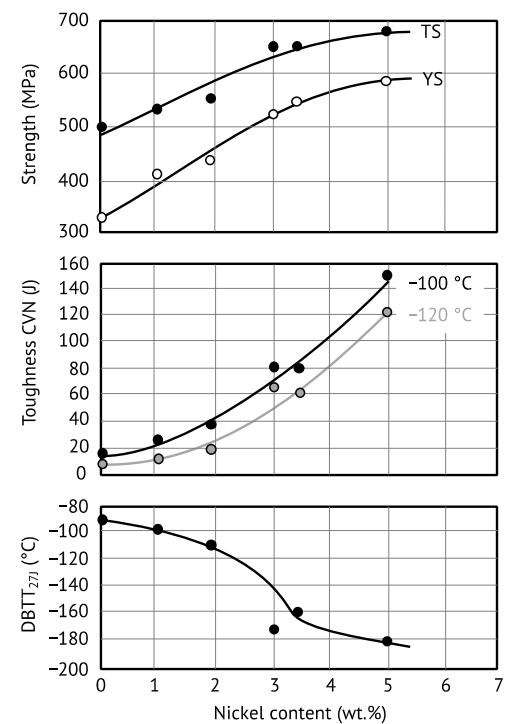


**Figure 15.** Influence of Ni content on the mechanical properties of cryogenic steels.

In recent years, toughness requirements towards 9% nickel steels have continuously increased due to growing safety demands (Figure 16) [92]. For instance, minimum notch impact values of 100 J or higher at −196 °C, noticeably exceeding the values specified by standards, are nowadays not uncommon. Consequently, the requirements regarding the degree of steel purity and in particular the phosphorous content, are also becoming sharper. Modern 9%Ni steels typically contain a maximum of 70 ppm phosphorous while further reduction to below 50 ppm P does not seem to bring significant toughness gains [95]. Otherwise, the evolution in alloy design and processing significantly contributes to performance improvement.

As discussed in Section 2.6, lowering the carbon content and refining the microstructure are major contributors to the improvement of low-temperature toughness in general, besides the direct effects related to nickel alloying. The processing schedule of 9%Ni steels inherently produces a fine-grained microstructure. Therefore, additional improvement potential mainly lies in further lowering the carbon content from the established range of 0.05–0.10 wt.% C to ultra-low levels of <0.03 wt.% C. Figure 17a demonstrates that reducing the carbon content from 0.050 to 0.025 wt.% results in increased impact energy at a test temperature of −196 °C as well as lower scattering. The ultra-low carbon content is particularly beneficial to the weld heat affected zone toughness (Figure 17b) providing a significant improvement especially in the intercritical heat affected zone, which experiences a peak metal temperature just below A<sub>c3</sub>. The reduced carbon content decreases the share of

residual metastable austenite that would otherwise mostly transform into brittle martensite upon cooling to cryogenic temperatures.

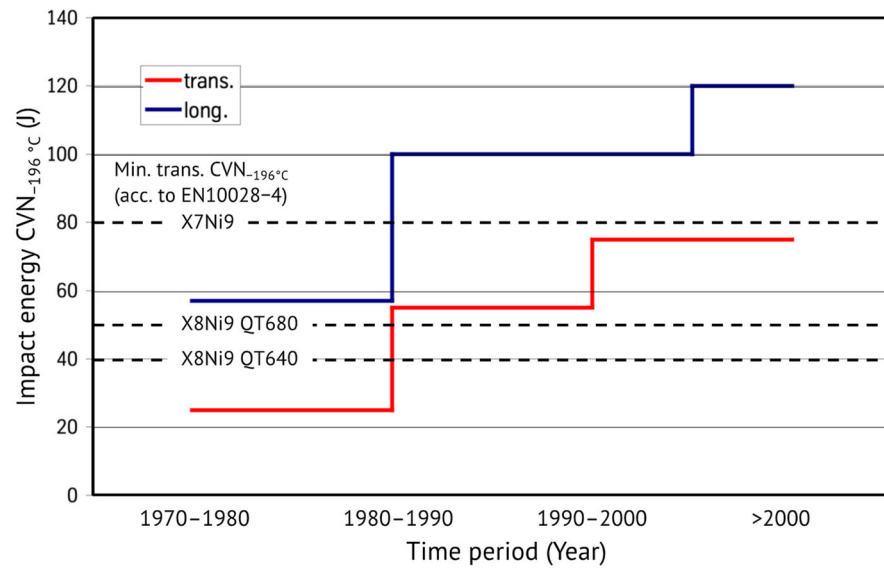


**Figure 16.** Evolution of market-driven toughness requirements for 9%Ni steel at  $-196\text{ }^{\circ}\text{C}$  in rolling and transverse direction (specified minimum toughness at  $-196\text{ }^{\circ}\text{C}$  acc. to EN10028-4 is represented by dashed lines).

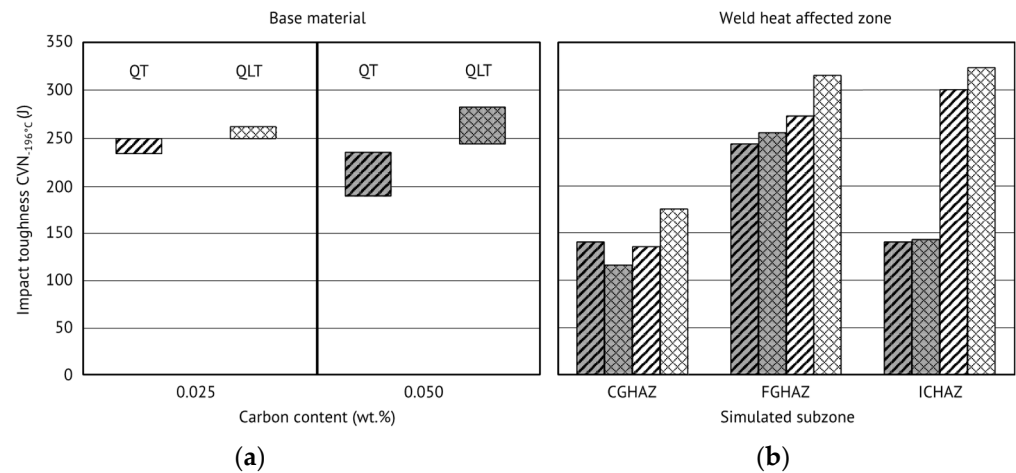


**Figure 17.** (a) Options for optimizing 9%Ni steel by reducing the carbon content and/or applying double quench and tempering (QLT). (b) Effect of these optimization on the properties of the weld heat affected zone.

The production of cryogenic steels necessarily involves heat treatment after hot rolling, in this instance quenching and tempering (Figure 18). This heat treatment can rely on air or water quenching, which may also be carried out in several stages. The heat treatment starts with re-heating the plate to above the  $A_{c3}$  temperature. After holding at that temperature, rapid cooling of the plate is achieved by using pressurized water. Tempering is undertaken in the temperature range of  $600\text{--}650\text{ }^{\circ}\text{C}$ . With increasing nickel content and the associated increase in the newly formed austenite during tempering, toughness raises equivalently. However, the pre-existing martensite and the newly formed austenite must be in a balanced ratio to each other. Above a certain tempering temperature, the formation of a high austenite content, being thermally less stable, results in a deterioration of toughness (cf. Figure 8).

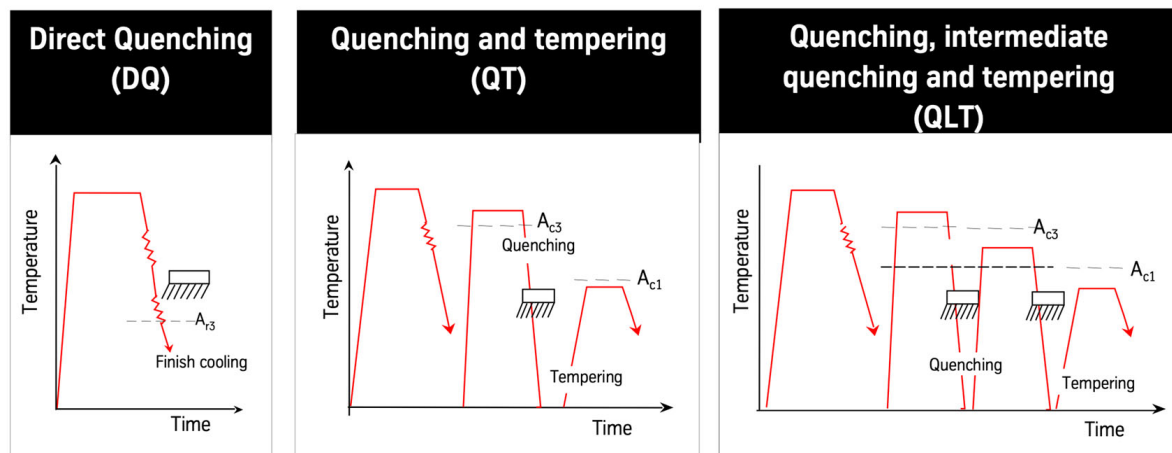


**Figure 18.** Heat treatment variants for the production of cryogenic steels with 5–9 wt.% Ni.

For highest demands regarding mechanical properties, double quenching can be adopted before tempering. Thereby the second quenching operation starts from a lower temperature in the intercritical ( $\alpha + \gamma$ ) phase field. This process variant, also called the quenching, lamellarizing and tempering (QLT) procedure, markedly enhances notch-toughness in the base steel as well as the weld heat affected zone (Figure 18). The QLT treatment aims to achieve a dense distribution of stable austenite precipitates. The Q step establishes a dislocated martensite structure within a small prior austenite grain size. The subsequent L step creates a fine-sized mixture of solute-rich and solute-poor martensite grains by partitioning austenite stabilizers, such as nickel and manganese, to the austenite grains formed in the intercritical temperature range. During the subsequent temper cycle, austenite nucleates readily along the boundaries of the alloy-enriched martensite laths. The QLT treatment is also suitable for upgrading 5.5%Ni steels for which not only too little but also thermally unstable austenite would be formed in a conventional QT treatment [96]. A modern process variant operates through direct quenching (DQ) from the rolling heat (Figure 18). Considering economic aspects, this method reduces energy cost by avoiding a separate reheating operation before quenching and also increases plant productivity. From a metallurgical point of view the major difference is that quenching is applied to deformed austenite (pancaked by hot rolling). This quenching condition can further contribute to microstructural refinement [59,97]. Tempering is performed as per the conventional QT process or after an optional lamellarizing treatment.

#### 4. Conclusions

Nickel alloying in carbon steels has many beneficial metallurgical functionalities either by itself or in combination with other alloying elements. This is due to the complex influence of nickel on the solid solution behavior of lattice defects in the iron crystal and on the mixed-phase thermodynamics. It must be emphasized that nickel has thus a consistently favorable effect and is therefore an increasingly important contributor to modern steel technology. Nickel's optimum use should be preferably defined within a holistic alloy design context in line with the applied processing conditions. This review has summarized the existing knowledge and experience of nickel alloying in carbon steels while research on the topic is proceeding, driven by the need for ever-increasing performance of steels. In particular, the ongoing global transition towards a green energy economy demands the superior properties of nickel alloyed carbon steels and, thus, represents a fast-growing market opportunity.

**Author Contributions:** Conceptualization, H.M. and A.K.; writing—review and editing, H.M. and A.K. All authors have read and agreed to the published version of the manuscript.

**Funding:** This research received no external funding.

**Conflicts of Interest:** The authors declare no conflict of interest.

## References

1. Lennon, J. *Nickel Outlook: Driven by Stainless Steel and Not Just Electric Vehicles*; Macquarie Capital Europe Ltd.: London, UK, 2021.
2. Rosenberg, S.J. *Nickel and Its Alloys*; US Department of Commerce, National Bureau of Standards: Washington, DC, USA, 1968; Volume 106.
3. Scott, H. Critical Ranges of Some Commercial Nickel Steels. *Sci. Pap. Bur. Stand.* **1920**, *16*, 195. [[CrossRef](#)]
4. Jesper, H.; Achtelik, K. *Kaltzähle Stähle*; International Nickel Deutschland: Düsseldorf, Germany, 1964.
5. Oikawa, H. Lattice Diffusion in Iron—A Review. *Tetsu-Hagane* **1982**, *68*, 1489–1497. [[CrossRef](#)] [[PubMed](#)]
6. Kang, B.Y.; Kim, H.J.; Hwang, S.K. Effect of Mn and Ni on the Variation of the Microstructure and Mechanical Properties of Low-Carbon Weld Metals. *ISIJ Int.* **2000**, *40*, 1237–1245. [[CrossRef](#)]
7. Cacciamani, G.; de Keyzer, J.; Ferro, R.; Klotz, U.E.; Lacaze, J.; Wollants, P. Critical Evaluation of the Fe–Ni, Fe–Ti and Fe–Ni–Ti Alloy Systems. *Intermetallics* **2006**, *14*, 1312–1325. [[CrossRef](#)]
8. Grong, O.; Matlock, D.K. Microstructural Development in Mild and Low-Alloy Steel Weld Metals. *Int. Met. Rev.* **1986**, *31*, 27–48. [[CrossRef](#)]
9. Bain, E.C. *Functions of the Alloying Elements in Steel*; US Steel Corporation: Pittsburg, PA, USA, 1939.
10. Portnoi, V.K.; Leonov, A.V.; Mudretsova, S.N.; Fedotov, S.A. Formation of Nickel Carbide in the Course of Deformation Treatment of Ni–C Mixtures. *Phys. Met. Metallogr.* **2010**, *109*, 153–161. [[CrossRef](#)]
11. Aall, N.H. Verschiebung Des Perlitpunktes Durch Nickel u. *Chrom. Stahl Und Eisen* **1924**, *44*, 256–259.
12. Krauss, G. Phases and Structures. In *Steels—Processing, Structure, and Performance*; Krauss, G., Ed.; ASM International: Almere, The Netherlands, 2015; pp. 17–38.
13. Ridley, N.; Malik, M.A.; Lorimer, G.W. Partitioning and Pearlite Growth Kinetics in an Ni–Cr Eutectoid Steel. *Mater. Charact.* **1990**, *25*, 125–141. [[CrossRef](#)]
14. Husby, H.; Iannuzzi, M.; Johnsen, R.; Kappes, M.; Barnoush, A. Effect of Nickel on Hydrogen Permeation in Ferritic/Pearlitic Low Alloy Steels. *Int. J. Hydrog. Energy* **2018**, *43*, 3845–3861. [[CrossRef](#)]
15. Eckstein, H.; Fennert, M.; Ohser, J. Application of Thermodynamic Computations to the Solution Behaviour of Niobium and Vanadium Carbonitrides. *Steel Res.* **1993**, *64*, 143–147. [[CrossRef](#)]
16. Sharma V K Lakshmanan, R.C.; Kirkaldy, J.S. Solubility of Niobium Carbide and Niobium Carbonitride in Alloyed Austenite and Ferrite. *Metall. Trans. A* **1984**, *15A*, 545–549. [[CrossRef](#)]
17. Kosazu, I. Overview of Accelerated Cooling of Plate. In *Proceedings of the International Conference on Accelerated Cooling of Steel*; Southwick, P.D., Ed.; The Metallurgical Society: Pittsburgh, PA, USA, 1986; pp. 15–31.
18. Imagumbai, M.; Nagumo, M. Fundamental Concept and Application of Accelerated Cooling Process. In *Proceedings of the International Conference on Accelerated Cooling of Steel*; Southwick, P.D., Ed.; The Metallurgical Society: Pittsburgh, PA, USA, 1986; pp. 297–312.
19. Müsgen, B. *Thyssen Technische Berichte*; Technical Report; Thyssen Stahl AG: Duisburg, Germany, 1982; pp. 71–85.
20. van Bohemen, S.M.C. Bainite and Martensite Start Temperature Calculated with Exponential Carbon Dependence. *Mater. Sci. Technol.* **2012**, *28*, 487–495. [[CrossRef](#)]
21. Borgenstam, A.; Hillert, M. Activation Energy for Isothermal Martensite in Ferrous Alloys. *Acta Mater.* **1997**, *45*, 651–662. [[CrossRef](#)]
22. Villa, M.; Somers, M.A.J. On the Role of Isothermal Martensite Formation during Cryogenic Treatment of Steels. *HTM J. Heat Treat. Mater.* **2020**, *75*, 49–72. [[CrossRef](#)]
23. Villa, M.; Somers, M.A.J. Thermally Activated Martensite Formation in Ferrous Alloys. *Scr. Mater.* **2018**, *142*, 46–49. [[CrossRef](#)]
24. Liu, Z.; Yu, Y.; Yang, J.; Wang, Z.; Guo, H.; Shang, C. Morphology and Crystallography Analyses of HSLA Steels with Hardenability Enhanced by Tailored C–Ni Collocation. *Metals* **2021**, *12*, 32. [[CrossRef](#)]
25. Huang, S.; Yu, Y.S.; Wang, Z.Q.; Su, S.; Chen, K.; Yuan, S.F.; Xie, Z.J.; Shang, C.J. Crystallographic Insights into the Role of Nickel on Hardenability of Wear-Resistant Steels. *Mater. Lett.* **2022**, *306*, 130961. [[CrossRef](#)]
26. Leslie, W.C. Iron and Its Dilute Substitutional Solid Solutions. *Metall. Mater. Trans. B* **1972**, *3*, 5–26. [[CrossRef](#)]
27. Hagi, H. Effect of Substitutional Alloying Elements on Diffusion Coefficient of Hydrogen in  $\alpha$ -Iron. *Mater. Trans. JIM* **1992**, *33*, 472–479. [[CrossRef](#)]
28. Ledbetter, H.M.; Reed, R.P. Elastic Properties of Metals and Alloys, I. Iron, Nickel, and Iron-Nickel Alloys. *J. Phys. Chem. Ref. Data* **1973**, *2*, 531–618. [[CrossRef](#)]
29. Morris, J.W., Jr.; Guo, Z.; Krenn, C.R.; Kim, Y.-H. The Limits of Strength and Toughness in Steel. *ISIJ Int.* **2001**, *41*, 599–611. [[CrossRef](#)]
30. Leslie, W.C.; Hornbogen, E. Physical Metallurgy of Steels. In *Physical Metallurgy*; Elsevier: Amsterdam, The Netherlands, 1996; pp. 1555–1620.
31. Okazaki, K. Solid-Solution Hardening and Softening in Binary Iron Alloys. *J. Mater. Sci.* **1996**, *31*, 1087–1099. [[CrossRef](#)]
32. Sato, A.; Meshii, M. Solid Solution Softening and Solid Solution Hardening. *Acta Metall.* **1973**, *21*, 753–768. [[CrossRef](#)]
33. Petukhov, B. Effect of Solid-Solution Softening of Crystalline Materials: Review. *Crystallogr. Rep.* **2007**, *52*, 112–122. [[CrossRef](#)]

34. Fine, M.E.; Vaynman, S.; Isheim, D.; Chung, Y.-W.; Bhat, S.P.; Hahin, C.H. A New Paradigm for Designing High-Fracture-Energy Steels. *Metall. Mater. Trans. A* **2010**, *41*, 3318–3325. [[CrossRef](#)]
35. Hildebrandt, U.; Dickenscheid, W. Plasticity and Alloy-Softening in Iron-Nickel-Alloys. *Acta Metall.* **1971**, *19*, 49–55. [[CrossRef](#)]
36. Chen, Y.T.; Atteridge, D.G.; Gerberich, W.W. Plastic Flow of Fe-Binary Alloys—I. A Description at Low Temperatures. *Acta Metall.* **1981**, *29*, 1171–1185. [[CrossRef](#)]
37. Lee, S.-J.; Lee, Y.-K. Quantitative Analyses of Ferrite Lattice Parameter and Solute Nb Content in Low Carbon Microalloyed Steels. *Scr. Mater.* **2005**, *52*, 973–976. [[CrossRef](#)]
38. Lee, S.-J.; Lee, Y.-K. Prediction of Austenite Grain Growth during Austenitization of Low Alloy Steels. *Mater. Des.* **2008**, *29*, 1840–1844. [[CrossRef](#)]
39. Hoerner, M.; Eberhart, M.; Speer, J. Ab-Initio Calculation of Solute Effects on Austenite Grain Boundary Properties in Steel. In Proceedings of the 3rd World Congress on Integrated Computational Materials Engineering—ICME 2015, Colorado Springs, CO, USA, 31 May–4 June 2015. [[CrossRef](#)]
40. Jin, H.; Elfimov, I.; Militzer, M. First-Principles Simulations of Binding Energies of Alloying Elements to the Ferrite-Austenite Interface in Iron. *J. Appl. Phys.* **2018**, *123*, 085303. [[CrossRef](#)]
41. Zurob, H.S.; Panahi, D.; Hutchinson, C.R.; Brechet, Y.; Purdy, G.R. Self-Consistent Model for Planar Ferrite Growth in Fe-C-X Alloys. *Metall. Mater. Trans. A* **2013**, *44*, 3456–3471. [[CrossRef](#)]
42. Yoshida, S.; Okumura, T.; Kita, H.; Takahashi, J.; Ushioda, K. High Temperature Tensile Properties and Its Mechanism in Low-Carbon Nb-Bearing Steels. *Mater. Trans.* **2014**, *55*, 899–906. [[CrossRef](#)]
43. Arioka, K.; Iijima, Y.; Miyamoto, T. Rapid Nickel Diffusion in Cold-Worked Carbon Steel at 320–450 °C. *Philos. Mag.* **2015**, *95*, 3577–3589. [[CrossRef](#)]
44. Marwick, A.D. Segregation in Irradiated Alloys: The Inverse Kirkendall Effect and the Effect of Constitution on Void Swelling. *J. Phys. F: Met. Phys.* **1978**, *8*, 1849–1861. [[CrossRef](#)]
45. Yonezawa, T.; Suzuki, K.; Ooki, S.; Hashimoto, A. The Effect of Chemical Composition and Heat Treatment Conditions on Stacking Fault Energy for Fe-Cr-Ni Austenitic Stainless Steel. *Metall. Mater. Trans. A* **2013**, *44*, 5884–5896. [[CrossRef](#)]
46. Ohkubo, N.; Miyakusu, K.; Uematsu, Y.; Kimura, H. Effect of Alloying Elements on the Mechanical Properties of the Stable Austenitic Stainless Steel. *ISIJ Int.* **1994**, *34*, 764–772. [[CrossRef](#)]
47. de Cooman, B.C.; Estrin, Y.; Kim, S.K. Twinning-Induced Plasticity (TWIP) Steels. *Acta Mater.* **2018**, *142*, 283–362. [[CrossRef](#)]
48. Shibata, K.; Seo, S.-J.; Kaga, M.; Uchino, H.; Sasanuma, A.; Asakura, K.; Nagasaki, C. Suppression of Surface Hot Shortness Due to Cu in Recycled Steels. *Mater. Trans.* **2002**, *43*, 292–300. [[CrossRef](#)]
49. Kondo, Y. Behaviour of Copper during High Temperature Oxidation of Steel Containing Copper Yasumitsu KONDO. *ISIJ Int.* **2004**, *44*, 1576–1580. [[CrossRef](#)]
50. Melford, D.A. The Influence of Residual and Trace Elements on Hot Shortness and High Temperature Embrittlement. *Philos. Trans. R. Soc. Lond. Ser. A Math. Phys. Sci.* **1980**, *295*, 89–103. [[CrossRef](#)]
51. Imai, N.; Komatsubara, N.; Kunishige, K. Effects of Cu and Other Tramp Elements on Steel Properties. Effect of Cu, Sn and Ni on Hot Workability of Hot-Rolled Mild Steel. *ISIJ Int.* **1997**, *37*, 217–223. [[CrossRef](#)]
52. Jiang, Y.; Xie, C. Evaluation Model of Susceptibility to Cu Hot Shortness of Cu-Containing LC Steel. *IOP Conf. Ser. Mater. Sci. Eng.* **2017**, *207*, 012098. [[CrossRef](#)]
53. Comineli, O.; Qaban, A.; Mintz, B. Influence of Cu and Ni on the Hot Ductility of Low C Steels with Respect to the Straightening Operation When Continuous Casting. *Metals* **2022**, *12*, 1671. [[CrossRef](#)]
54. Ghosh, A.; Chatterjee, S.; Mishra, B.; Das, S. Microstructure, Properties, and Age Hardening Behavior of a Thermomechanically Processed Ultralow-Carbon Cu-Bearing High-Strength Steel. *Metall. Mater. Trans. A* **2005**, *36*, 703–713. [[CrossRef](#)]
55. Zhang, C.; Enomoto, M. Study of the Influence of Alloying Elements on Cu Precipitation in Steel by Non-Classical Nucleation Theory. *Acta Mater.* **2006**, *54*, 4183–4191. [[CrossRef](#)]
56. Vaynman, S.; Isheim, D.; Prakash Kolli, R.; Bhat, S.P.; Seidman, D.N.; Fine, M.E. High-Strength Low-Carbon Ferritic Steel Containing Cu-Fe-Ni-Al-Mn Precipitates. *Metall. Mater. Trans. A* **2008**, *39*, 363–373. [[CrossRef](#)]
57. Jiao, Z.B.; Luan, J.H.; Zhang, Z.W.; Miller, M.K.; Ma, W.B.; Liu, C.T. Synergistic Effects of Cu and Ni on Nanoscale Precipitation and Mechanical Properties of High-Strength Steels. *Acta Mater.* **2013**, *61*, 5996–6005. [[CrossRef](#)]
58. Rinebolt, J.A.; Harris, W.J. Effect of Alloying Elements on Notch Toughness of Pearlitic Steels. *Trans. Am. Soc. Met.* **1951**, *43*, 1175–1214.
59. Mohrbacher, H. Property Optimization in As-Quenched Martensitic Steel by Molybdenum and Niobium Alloying. *Metals* **2018**, *8*, 234. [[CrossRef](#)]
60. Mohrbacher, H. Metallurgical Effects of Niobium and Molybdenum on Heat-Affected Zone Toughness in Low-Carbon Steel. *Appl. Sci.* **2019**, *9*, 1847. [[CrossRef](#)]
61. Morris, J.W., Jr. On the Ductile-Brittle Transition in Lath Martensitic Steel. *ISIJ Int.* **2011**, *51*, 1569–1575. [[CrossRef](#)]
62. Hanamura, T.; Torizuka, S.; Tamura, S.; Enokida, S.; Takechi, H. Effect of Austenite Grain Size on Transformation Behavior, Microstructure and Mechanical Properties of 0.1C–5Mn Martensitic Steel. *ISIJ Int.* **2013**, *53*, 2218–2225. [[CrossRef](#)]
63. Gerberich, W.W.; Chen, Y.T.; Atteridge, D.G.; Johnson, T. Plastic Flow of Fe-Binary Alloys—II. Application of the Description to the Ductile-Brittle Transition. *Acta Metall.* **1981**, *29*, 1187–1201. [[CrossRef](#)]

64. Tanaka, M.; Matsuo, K.; Yoshimura, N.; Shigesato, G.; Hoshino, M.; Ushioda, K.; Higashida, K. Effects of Ni and Mn on Brittle-to-Ductile Transition in Ultralow-Carbon Steels. *Mater. Sci. Eng. A* **2017**, *682*, 370–375. [[CrossRef](#)]
65. Müsgen, B. Kaltzähe Nickelstähle. *Thyssen Tech. Ber.* **1982**, *1*, 71–85.
66. Kern, A.; Kirschbaum, M.; Kucharczyk, P.; Langenberg, P.; Schnitter, F. Bewertung Des Spröbruchwiderstands Höchstfester Stähle Im Mobilkranbau. *Stahlbau* **2022**, *91*, 211–220. [[CrossRef](#)]
67. Wallin, K. *Fracture Toughness of Engineering Materials: Estimation and Application*; EMAS Publishing: Warrington, UK, 2011; ISBN 978-0-9552994-6-9, 0-955-299-462.
68. Jarvis, A.R.; Bulloch, J.H. The Effect of Nickel Content on the Environmental Assisted Cracking (EAC) Behaviour of Low Alloy Steels in Sour Environments—A Review. *Int. J. Press. Vessel. Pip.* **1992**, *49*, 271–307. [[CrossRef](#)]
69. ISO 15156-2:2020 Petroleum and Natural Gas Industries—Materials for Use in H<sub>2</sub>S-Containing Environments in Oil and Gas Production—Part 2: Cracking-Resistant Carbon and Low-Alloy Steels, and the Use of Cast Irons. 2015. Available online: <https://www.iso.org/standard/66641.html> (accessed on 30 November 2022).
70. Kappes, M.; Iannuzzi, M.; Rebak, R.B.; Carranza, R.M. Sulfide Stress Cracking of Nickel-Containing Low-Alloy Steels. *Corros. Rev.* **2014**, *32*, 101–128. [[CrossRef](#)]
71. Iino, M.; Nomura, N.; Takezawa, H.; Takeda, T. Engineering Solutions to the H<sub>2</sub>S Problem in Linepipes. In *Current Solutions to Hydrogen Problems in Steels*; Interrante, C.G., Pressouyre, G.M., Eds.; American Society for Metals: Washington, DC, USA, 1982; pp. 159–167.
72. Hui, W.; Zhang, H.; Zhang, Y.; Zhao, X.; Shao, C. Effect of Nickel on Hydrogen Embrittlement Behavior of Medium-Carbon High Strength Steels. *Mater. Sci. Eng. A* **2016**, *674*, 615–625. [[CrossRef](#)]
73. Mohrbacher, H.; Senuma, T. Alloy Optimization for Reducing Delayed Fracture Sensitivity of 2000 MPa Press Hardening Steel. *Metals* **2020**, *10*, 853. [[CrossRef](#)]
74. Kim, S.J.; Hwang, E.H.; Park, J.S.; Ryu, S.M.; Yun, D.W.; Seong, H.G. Inhibiting Hydrogen Embrittlement in Ultra-Strong Steels for Automotive Applications by Ni-Alloying. *Npj Mater. Degrad* **2019**, *3*, 12. [[CrossRef](#)]
75. Park, J.S.; Seong, H.G.; Hwang, J.; Kim, S.J. Adverse Effects of Ni on the Mechanical and Corrosion-Induced Hydrogen Embrittlement Properties of Ultra-Strong Giga Steel Used for Automotive Applications. *Mater. Des.* **2020**, *193*, 108877. [[CrossRef](#)]
76. Solana, F.; Takamada, C.; Bernstein, I.M.; Thompson, W. The Role of Retained Austenite in Stress Corrosion Cracking of Steels. *Metall. Trans. A* **1991**, *18*, 1023–1028. [[CrossRef](#)]
77. Takasawa, K.; Wada, Y.; Ishigaki, R.; Kayano, R. Effects of Grain Size on Hydrogen Environment Embrittlement of High Strength Low Alloy Steel in 45 MPa Gaseous Hydrogen. *Mater. Trans.* **2010**, *51*, 347–353. [[CrossRef](#)]
78. Tobler, R.; Cheng, Y.-W. Midrange Fatigue Crack Growth Data Correlations for Structural Alloys at Room and Cryogenic Temperatures. In *Fatigue at Low Temperatures*; ASTM International: West Conshohocken, PA, USA, 1985; pp. 5–30.
79. Park, J.Y.; Kim, B.K.; Nam, D.G.; Kim, M.H. Effect of Nickel Contents on Fatigue Crack Growth Rate and Fracture Toughness for Nickel Alloy Steels. *Metals* **2022**, *12*, 173. [[CrossRef](#)]
80. You, Y.; Shang, C.; Subramanian, S. Effect of Ni Addition on Toughness and Microstructure Evolution in Coarse Grain Heat Affected Zone. *Met. Mater. Int.* **2014**, *20*, 659–668. [[CrossRef](#)]
81. Huang, G.; Wan, X.; Wu, K.; Zhao, H.; Misra, R. Effects of Small Ni Addition on the Microstructure and Toughness of Coarse-Grained Heat-Affected Zone of High-Strength Low-Alloy Steel. *Metals* **2018**, *8*, 718. [[CrossRef](#)]
82. Wang, Z.Q.; Wang, X.L.; Nan, Y.R.; Shang, C.J.; Wang, X.M.; Liu, K.; Chen, B. Effect of Ni Content on the Microstructure and Mechanical Properties of Weld Metal with Both-Side Submerged Arc Welding Technique. *Mater. Charact.* **2018**, *138*, 67–77. [[CrossRef](#)]
83. Liu, J.; Sun, J.; Wei, S.; Lu, S. The Effect of Nickel Contents on the Microstructure Evolution and Toughness of 800 MPa Grade Low Carbon Bainite Deposited Metal. *Crystals* **2021**, *11*, 709. [[CrossRef](#)]
84. Zhang, Z.; Farrar, R. Influence of Mn and Ni on the Microstructure and Toughness of C-Mn-Ni Weld Metals. *Weld. Res. Suppl.* **1997**, *76*, 183–196.
85. Keehan, E.; Karlsson, L.; Andrén, H.-O. Influence of Carbon, Manganese and Nickel on Microstructure and Properties of Strong Steel Weld Metals: Part 1—Effect of Nickel Content. *Sci. Technol. Weld. Join.* **2006**, *11*, 1–8. [[CrossRef](#)]
86. Heisterkamp, F.; Hulka, K. Low-Carbon Mn-Ni-Nb Steel: Part 1 Development for Pipeline Applications Using Relaxed Rolling Conditions. *Met. Technol.* **1984**, *11*, 535–544. [[CrossRef](#)]
87. Piette, M.; Dubrulle-Prat, E.; Perdrix, C.; Schwinn, V.; Streisselberger, A.; Hulka, K. Effect of 0–0.1%Nb Additions on Mechanical Properties of Plates Processed by Thermomechanically Controlled Processing and Accelerated Cooling. *Ironmak. Steelmak.* **2001**, *28*, 175–179. [[CrossRef](#)]
88. Mohrbacher, H. Mo and Nb Alloying in Plate Steels for High-Performance Applications. In *Proceedings of the 1st International Symposium on the Recent Developments in Plate Steels*; AIST: Winter Park, CO, USA, 2011; pp. 169–179.
89. Mohrbacher, H. Reverse Metallurgical Engineering towards Sustainable Manufacturing of Vehicles Using Nb and Mo Alloyed High Performance Steels. *Adv. Manuf.* **2013**, *1*, 28–41. [[CrossRef](#)]
90. Grill, R.; Schimböck, R.; Heigl, G. Recent Results from Clad Plate Production. In *Recent Advances of Niobium Containing Materials in Europe*; Hulka, K., Klinkenberg, C., Mohrbacher, H., Eds.; Verlag Stahleisen: Düsseldorf, Germany, 2005; pp. 81–106.

91. Schwinn, V.; Flüß, P.; Ormston, D. Low Carbon Bainitic TMCP Plate for Structural and Line-Pipe Application. In *Recent Advances of Niobium Containing Materials in Europe*; Hulka, K., Klinkenberg, C., Mohrbacher, H., Eds.; Verlag Stahleisen: Düsseldorf, Germany, 2005; pp. 43–58.
92. Hickmann, K.; Kern, A.; Schriever, U.; Stumpfe, J. Production and Properties of High-Strength Nickel-Alloy Steel Plates of Low Temperature Applications. In Proceedings of the 1st International Conference Super-High Strength Steels, Rome, Italy, 2–4 November 2005.
93. Moriyama, K.; Yoshimura, H.; Kaku, K. High-Toughness Heavy Section Steel Plate with Minimum Yield Strength of 900 MPa for Deep Submergible Vehicle. *Trans. Iron Steel Inst. Jpn.* **1983**, *23*, 434–439. [[CrossRef](#)]
94. Hoshino, M.; Muraoka, H.; Saitoh, N.; Saeki, O. Development of Super-9%Ni Steel Plates with Superior Low-Temperature Toughness for LNG Storage Tanks. *Nippon Steel Tech. Rep.* **2004**, *90*, 20–24.
95. Furukimi, O.; Saito, Y. The Effects of Grain Boundary Phosphorus Segregation and Heat Treatment on Toughness of 9% Ni Steel and Its Welded Joint. *ISIJ Int.* **1990**, *30*, 390–396. [[CrossRef](#)]
96. Kim, J.I.; Syn, C.K.; Morris, J.W. Microstructural Sources of Toughness in QLT-Treated 5. 5Ni Cryogenic Steel. *Metall. Trans. A* **1983**, *14*, 93–103. [[CrossRef](#)]
97. Zurutuza, I.; Isasti, N.; Detemple, E.; Schwinn, V.; Mohrbacher, H.; Uranga, P. Effect of Quenching Strategy and Nb-Mo Additions on Phase Transformations and Quenchability of High-Strength Boron Steels. *JOM* **2021**, *73*, 3158–3168. [[CrossRef](#)]

**Disclaimer/Publisher’s Note:** The statements, opinions and data contained in all publications are solely those of the individual author(s) and contributor(s) and not of MDPI and/or the editor(s). MDPI and/or the editor(s) disclaim responsibility for any injury to people or property resulting from any ideas, methods, instructions or products referred to in the content.